REPORT DOCUMENTATION PAGE

AFRL-SR-BL-TR-98-

G426

1. AGENCY USE ONLY (Leave blank)	2. REPORT DATE	3. REPORT TYPE AND DATES COVERED
		Final 01 Feb 95 to 31 Jan 98

4. TITLE AND SUBTITLE
Fabrication of Self-Supporting ALN Single Film Substrates by Van Der Waals Lift-Off

5. FUNDING NUMBERS
61102F
2305/ES

6. AUTHOR(S)
Professor Ohunchi

7. PERFORMING ORGANIZATION NAME(S) AND ADDRESS(ES)

University of Washington
3935 University Way, NE
Seattle WA 98105-6613

8. PERFORMING ORGANIZATION REPORT NUMBER

9. SPONSORING/MONITORING AGENCY NAME(S) AND ADDRESS(ES)

AFOSR/NE
110 Duncan Ave RmB115
Bolling AFB DC 20332-8050

10. SPONSORING/MONITORING AGENCY REPORT NUMBER

F49620-95-1-0142

19980514 113

11. SUPPLEMENTARY NOTES

12a. DISTRIBUTION/AVAILABILITY STATEMENT

APPROVAL FOR PUBLIC RELEASED, DISTRIBUTION UNLIMITED

12b. DISTRIBUTION CODE

13. ABSTRACT (Maximum 200 words)

The goal of the project was to develop a method to fabricate a free aluminum nitride (AIN) thin films. This was developed by growing AIN thin films on top of layered tungsten sulfide (WS2) thin films which were deposited on a mechanically rigid substrate material such as Si and Al2o3, followed by mechanical specation of AIN thin films thorough the inter-layers of WS2. This project involved the design and construction of a cold wasll metal organic chemical vapor deposition (MOCVD) for WS2 thin films, and the AIN thin film deposition by atomic layer growth (ALG) process. WS2 thin films were deposited using the reaction of H2S with W(CO)6. Microstructure for WS2 thin films is generally characterized by the formation of crystallites with basal planes parallel to the interface for the first few tens of nanometers, followed by the formation of crystallites with their basal planes non-parallel to the substrate. Process conditions to grow AIN thin films via ALG using dimethylamine-alane (DMEAA) and ammonia (NH3) were investigated. Close proximity of the lattice constant of WS2 to those of AIN lead to a potential application of this materials as a substrate for subsequent growth of AIN, however, the lift-off process was severely dependent on the microstructure of WS2 interlayers.

17. SECURITY CLASSIFICATION OF REPORT	18. SECURITY CLASSIFICATION OF THIS PAGE	19. SECURITY CLASSIFICATION OF ABSTRACT	20. LIMITATION OF ABSTRACT
UNCLASSIFIED	UNCLASSIFIED	UNCLASSIFIED	UL

DTIC QUALITY INSPECTED 4

Final Report Submitted to the

Air Force Office of Scientific Research

Fabrication of AlN Thin Film Substrates by "van der Waals Lift-off Technique"

UNIVERSITY OF WASHINGTON

Fumio S. Ohuchi
Department of Materials Science and Engineering
BOX 352120
Seattle, WA 98195

Tel # (206) 685-8272
Fax # (206) 543-3100
e-mail: ohuchi@u.washington.edu

April 29, 1998

Final Report to Air Force Office of Scientific Research

AFOSR/NE 110 Duncan Avenue, Suite B115 Bolling AFB
Washington, D.C. 20332-0001

Program Manager: Major Mike Prairie

Fabrication of AlN Thin Film Substrates by "van der Waals Lift-off Technique"

Principal Investigator: Fumio S. Ohuchi

Department of Materials Science and Engineering
The University of Washington
BOX 352120
Seattle, WA 98195

Tel # (206) 685-8272
Fax # (206) 543-3100
e-mail: ohuchi@u.washington.edu

Unlimited

The goal of the project was to develop a method to fabricate a free aluminum nitride (AlN) thin films. This was developed by growing AlN thin films on top of layered tungsten sulfide (WS_2) thin films which were deposited on a mechanically rigid substrate material such as Si and Al_2O_3, followed by mechanical separation of AlN thin films thorough the inter-layers of WS_2. This project involved the design and construction of a cold wall metal organic chemical vapor deposition (MOCVD) for WS_2 thin films, and the AlN thin film deposition by atomic layer growth (ALG) process. WS_2 thin films were deposited using the reaction of H_2S with $W(CO)_6$. Microstructure for WS_2 thin films is generally characterized by the formation of crystallites with basal planes parallel to the interface for the first few tens of nanometers, followed by the formation of crystallites with their basal planes non-parallel to the substrate. Process conditions to grow AlN thin films via ALG using dimethylamine-alane (DMEAA) and ammonia (NH_3) were investigated. Close proximity of the lattice constant of WS_2 to those of AlN lead to a potential application of this materials as a substrate for subsequent growth of AlN, however, the lift-off process was severely dependent on the microstructure of WS_2 interlayers.

TABLE OF CONTENTS

List of Tables

List of Figures

I. INTRODUCTION AND OBJECTIVES

This report is the final summary for AFSOR project No. Grant No. F49620-95-1-0142 entitled "Fabrication of AlN Thin Film Substrates by van der Waals Lift-off Technique".

The project was aimed at overcoming one of the major obstacles to research in III-Nitride materials arising from a lack of suitable substrate materials that were lattice matched and thermally compatible with the III-Nitrides. From the thin film growth, an ideal solution is to use a same kind of III-Nitride material in its intrinsic form as a substrate for subsequent growth of the III-Nitrides. The goal of the project was to develop a novel method to fabricate a free standing III-Nitride thin films so as to use as a substrate for further growth of the III-Nitride materials.

In our experimental program, this was developed by growing aluminum nitride (AlN) thin films on top of layered tungsten sulfide (WS_2) thin films which were deposited on a mechanically-rigid substrate material such as silicon and alumina. Choice of the material combination was based on the fact that the WS_2 crystallized into a layered structure with the lattice constant (a = 3.15 Å) remarkably close to that of AlN (a = 3.11 Å). The layered WS_2 thin films can be deposited on any material via a process called "van der Waals epitaxy (VDWE)". The crystalline structure of WS_2 is shown in Fig. 1. Bonding within the WS_2 layer is strongly covalent while each layer is held via weak van der Waals (VDW) interaction, so that AlN thin films that are deposited on the WS_2 can be mechanically separated from the substrate by cleaving thorough the inter-layers of WS_2. This concept is illustrated in Fig. 2.
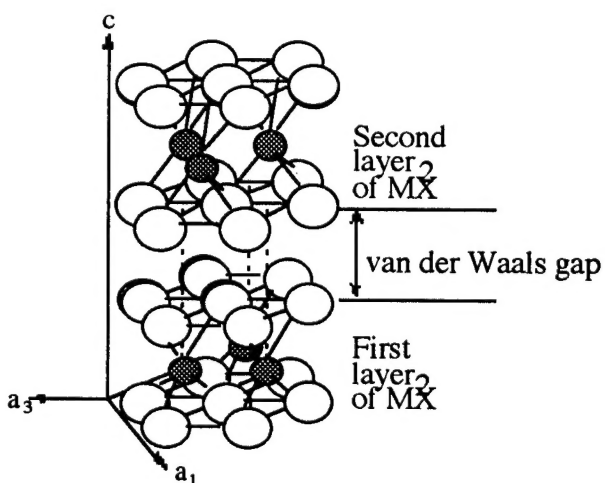
Figure 1.   Crystal structure of WS_2
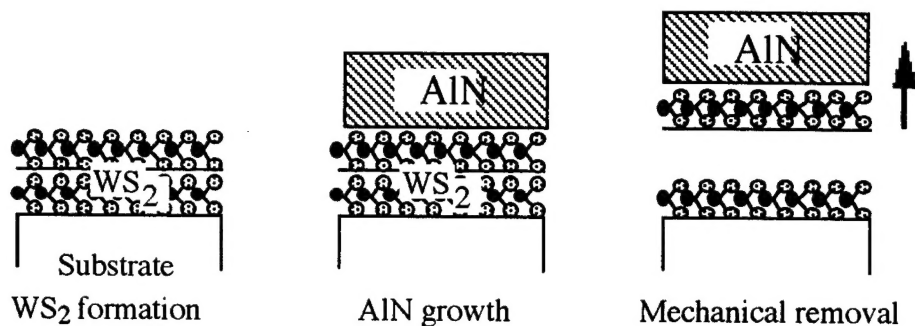
Fig.2 Schematic illustration of fabrication of AlN free standing substrate

Our objectives were to:

- Develop an appropriate technique to growth WS_2 in thin film forms on rigid substrate materials
- Optimize the deposition process
- Develop a process to grow AlN on top of the WS_2 thin films
- Separate AlN thin films from the substrate.

We called this process, "van der Waals lift-off technique (VDWLT)".

II. SPECIFIC TASKS FOR THE PROJECT

Specific experimental tasks that were accomplished in this project are listed below:

A. Synthesis and evaluation of bulk WS_2 single crystalline substrates
B. Development of the synthetic technique to fabricate WS_2 layered thin films
C. Characterization of the WS_2 layered thin films
D. Development of the process to deposit AlN thin film on the WS_2 substrate materials.
E. Demonstration of the van der Waals lift-off technique

III. SUMMARY OF WORK

A layered single crystal of WS_2 was synthesized using an iodine transport method in a quartz ampoule. Single crystals with size ranging from $4x6x0.2$ mm^3 to $12x10x0.3$ mm^3 were obtained, and their crystal structure was identified as hexagonal (P63/mmc) by x-ray diffraction.

The formation of WS_2 thin films on Si (100) was studied using H_2S and $W(CO)_6$ as the precursors in an metal-organic chemical vapor deposition (MOCVD) arrangement. Highly

-6-

crystalline WS_2 thin films were successfully prepared. Various spectroscopic evidences revealed that the structural quality was at least similar to that of the single crystalline WS_2. The crystalline orientation, however, was strongly dependent on the deposition conditions. A parameter to distinguish the degree of preferred orientation was introduced based on x-ray diffraction peak intensity and full-width-at-maximum (FWHM), and was found to be very useful in evaluating the effects of the experimental conditions for the structure of the thin films. The present study showed that MOCVD was clearly a feasible technique for growing WS_2 thin films, and the technique possessed a number of advantages over more conventional deposition processes, such as sputtering, ion beam sputtering, etc. A high deposition rate (average 20 nm/min) while maintaining a high degree of preferred orientation was particularly promising. The microstructure for MOCVD-grown WS_2 thin films was generally characterized by the formation of crystallites with basal planes parallel to the interface for the first few tens of nanometers, followed by the formation of crystallites with basal planes non-parallel to the substrate. Cross-sectional high resolution electron microscopy revealed that the transition in the microstructure from parallel to non-parallel orientation occurred smoothly, showing that the WS_2 lattice was bent and curved. Raman scattering was applied to study the effects of lattice curvature and orientation in WS_2 thin films. As the fraction of crystallites with their basal plane non-parallel to the interface increases in the thin film structure, a large second order Raman peak appeared as a shoulder of the A_{1g} mode at lower wavenumbers. This peak was characterized by two phonon-coupling originating from longitudinal acoustic (LA) and transverse acoustic (TA) phonons at the K point of the Brillouin zone. The occurrence of the localized curvature in the thin film microstructure was responsible for the enhancement of this unique second-order-Raman (SOR) effect. A great deal of new information about the growth of WS_2 thin films as well as microstructure-property relationship was obtained from this study.

Subsequent deposition of aluminum nitride (AlN) thin films on WS_2 thin films was investigated. This was done in a commercial MOCVD reactor using a newly developed process called "Atomic Layer Growth (ALG)". In this process, the AlN films were deposited by sequentially switching the gas flow between a metalorganic precursor, dimethylamine alane (DEMAA), and NH_3 with a hydrogen flush step between each precursor step. This process was carried out at atmospheric pressure, and demonstrated self-limiting growth over a narrow temperature range. For the deposition of AlN on WS_2 substrate, a range of processing parameters was extremely narrow as compared to Si and Al_2O_3 materials; nevertheless the deposition procedure for the AlN growth on WS_2 was established at 723°K with the reactor pressure ranging from 25 to 100 torr using ALG sequence called "4-5-4-5" process. Propensity of DMEAA molecules to form involatile solid with oxygen is relatively high, whereas WS_2 surface contains no or little oxygen, making it difficult for DMEAA molecules to initiate the surface-reaction. Although a sulfur is among the family including an oxygen, the chemistry of DMEAA to sulfur seems to be very different from that to oxygen, which leaves this issue as the future study. Crystalline films deposited on WS_2 thin films showed a preferred AlN(0001) orientation, where the microstructure of the films was dependent on the microstructure of the substrate WS_2 thin

films. Detailed characterization of thin film structure was made by high resolution electron microscopy. Van der Waals lift-off was demonstrated from $AlN/WS_2/Si$ specimens. A portion of AlN thin film was characterized by SEM and TEM. Inability to fabricate thick enough specimens of the AlN thin film by ALG technique limited further investigation of this process.

III. EXPERIMENTAL DETAILS

A. SYNTHESIS AND EVALUATION OF BULK WS_2 SINGLE CRYSTALLINE SUBSTRATES.

The chemical vapor transport method using halogen as a transport agent in a quartz ampoule is a common technique for the synthesis of metal dichalcogenide single crystals [1-3]. The growth conditions, however, are strongly dependent on the type of materials to be grown, the amount of halogens, ampoule shape and size, temperature gradient in the furnace, temperature stability, etc. There is, therefore, no standard recipe for the growth available. Specific conditions for each growth must be obtained and optimized.

WS_2 powder (Johnson Matthey Chemicals, Lot 11829, 99.8% purity) was used as a starting material for the growth of single crystalline tungsten disulfide. As a transport agent, we have chosen iodine (Johnson Matthey Chemicals, Lot 10619, 99.999% purity) because of its solid phase stability and fast transport kinetics at ambient temperature, as well as the ease of material handling. The powdered compound was first introduced into a fused quartz ampoule (22.5mm inner diameter and 180mm length). The weight of I_2 incorporated in the ampoule (mg per cm^{-3} of ampoule) is a critical parameter affecting the crystal quality of the resultant products and must be determined experimentally. The ampoule was evacuated to a pressure less than 10^{-3} torr, during which the ampoule was partly immersed in a liquid nitrogen to avoid possible loss of I_2 by evaporation. This process was repeated three times before sealing off the ampoule by constriction with a propane torch. The ampoule was then loaded into a three-zone furnace (Lindberg 54357-A), such that the ampoule containing the source materials was at the hottest point in the furnace and the other end was at a slightly lower temperature, thereby creating a temperature gradient within the ampoule. The temperature gradient was maintained within $\pm 2°C$ during the period of single crystal growth.

The growth conditions are shown in Table 1. At the end of each growth period, the ampoule was quickly removed from the furnace and quenched to room temperature. This process results in condensation of the vaporized I_2 within the ampoule and prevents its incorporation into the crystals. The obtained crystals were black and shiny and consisted of hexagonal sheets stacked together. The size of crystals were in the range of $\sim 4x6x0.2$ mm^3 and $\sim 12x10x0.3$ mm^3.

An x-ray diffractometer (Phillips PW1830) with Cu-Ka radiation was used to characterize the crystal structure. The crystal was identified as the hexagonal 2H type. In the tungsten-sulfur system, there are two well-established compounds known as WS_2 and WS_3, however no WS_3 was present in our products. The crystal from ampoules with higher iodine concentration (7mg/cm-3) formed mostly a hexagonal structure, whereas the crystals from ampoules with a lower iodine concentration (5mg/cm-3) formed hexagonal structure as a main phase, but co-existed with rhombohedral phase. X-ray diffraction patters obtained from the 2H-WS2 indicated a series of Miller indices as (0002), (0004), (0006), (0008) etc., suggesting that the (001) planes are preferably oriented along the basal plane.

Table 1 : Growth conditions for WS_2 single crystals

Run #	Mass of I_2 per unit volume of ampoule	Temperature distribution T_H T_L(°C)		Growth duration	Appearance	Crystal size (average)
#1	5.0 mg/cm^3	910	830	14 days	flat plate, lump of small crystals	3 x 3 mm^2
#2	7.0 mg/cm^3	910	865	30 days	hexagonal sheet	7 x 6mmm^2
#3	5.6 mg/cm^3	905	865	38 days	hexagonal sheet	8 x 8 mm^2

B.   DEVELOPMENT OF THE SYNTHETIC TECHNIQUE TO FABRICATE WS$_2$ LAYERED THIN FILMS

B.1   SELECTION OF TECHNIQUE

There are a number of techniques to prepare layered materials like WS_2 thin films; those are RF-sputtering [4], ion beam sputtering [5] , and pulsed laser beam deposition [6]. Metal organic chemical vapor deposition (MOCVD) is, however, the least explored for this kind of materials. Owing to the versatility of MOCVD for high growth rates, high throughput, and the ability to use a wide range of metal-organic precursors, the MOCVD method was chosen to synthesize the WS_2 thin films.

B.2   MOCVD APPARATUS

The MOCVD apparatus that was used in the present research was specifically designed and constructed. The system diagram is shown in Fig. 3.
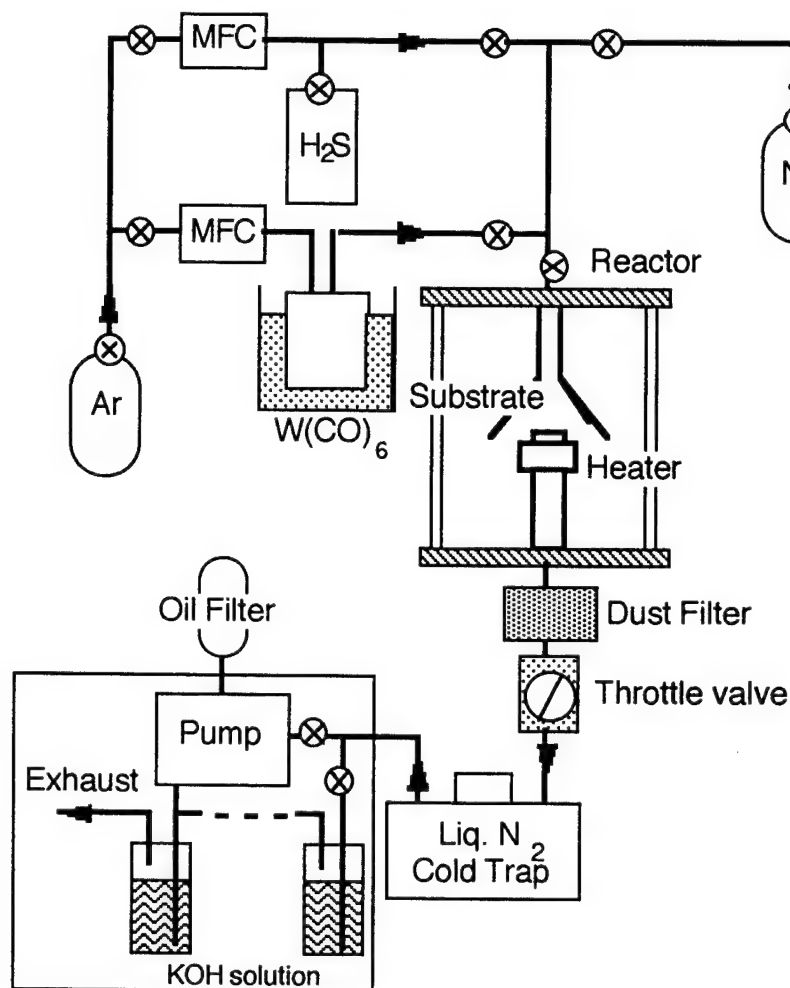
Fig. 3 Schematic diagram of MOCVD system for WS$_2$ thin film deposition

For the deposition of tungsten disulfide (WS$_2$), tungsten hexacarbonyl (W(CO)$_6$, Johnson Matthey, 99%) and hydrogen sulfide (H$_2$S, Matheson, 99.5%) were used as sources based on the following chemical reaction.

$$W(CO)_6 + 2H_2S \longrightarrow WS_2 + 6CO + 2H_2$$
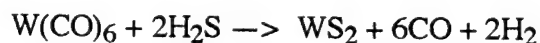
H$_2$S is fed into a gas line with pressure regulated between 7×10^3 and 4.2×10^4 Pa, and W(CO)$_6$ is evaporated in a bubbler immersed in a constant heat bath. The solid phase W(CO)$_6$ was chosen because of its easy treatment and pyrolysis into molecules at low temperatures. Both sources were transported with dry Ar carrier gas with the flow rates, Ar(H$_2$S) and Ar(W(CO)$_6$) independently controlled by a multichannel mass flow meter (MKS-135901). Typically, 40% H$_2$S and W(CO)$_6$ of which vapor pressure is 2.3×10^2 Pa at T$_{bubbler}$ = 343K are mixed in Ar streams. The flow rate ratio, Ar(H$_2$S)/Ar(W(CO)$_6$), was kept unchanged while the reactor pressure was changed. A

maximum flow rate of 1000 sccm full scale with 0.5% accuracy can be achieved. Source materials were mixed just prior to being fed into the reactor.

The reactor consists of a gas inlet funnel and a substrate holder and heater, which are housed in a cylindrically-shaped reactor made of fused quartz (an inner diameter of 100 mm and a length of 380 mm). A vertical reactor was adopted because of its advantage in obtaining asymmetric flow patterns, in which the flow becomes three-dimensional with no azimuthal gradients, resulting in better surface uniformity [7]. The substrate was radiatively heated from the backside using a small halogen lamp, capable of heating the substrate to 900K. Temperature was measured with K-type thermocouples directly attached to the surface of substrate. Pressure in the reactor was maintained in the range of 0.3 ~ 2.6 Pa, monitored by a capacitance manometer (MKS-112A01).

The exhaust system consists of a throttle valve, a liquid N_2 cold trap, a mechanical pump, and an absorber. During the experiments, exhaust H_2S and reaction by-products are condensed on the walls of the liquid N_2 cold trap. At the end of the deposition cycle, the cold trap is isolated from the rest of the MOCVD system, warms up to vaporize the condensed species. Vaporized species are forced to pass through several stages of strong KOH solution for neutralization. N_2 gas is used to purge the remnant reactant gases in the tubes and reactor. Since inhalation of H_2S can lead to loss of olfactory perception, laboratory personnel might not even be aware of its presence. The laboratory is equipped with permanent air monitor (Industrial Scientific Corporation) which gives an alarm if the H_2S concentration ever exceeds the work place safe limit (10 ppm). As an extra precaution, personal gas badges were supplied to the personnel working in the laboratory.

B.3 WS$_2$ THIN FILM GROWTH PROCEDURE

Commercially available well polished single crystalline (100) Si and (0001)Al$_2$O$_3$ wafers were used as the substrate material. With these materials, effects of the surface roughness and inhomogeneity of substrate materials on the growth of WS$_2$ thin films can be minimized. In addition, naturally grown SiO$_2$ layers may isolate potential chemical interactions with the Si substrate material. A standard cleaning procedure, including 1-1-1 trichloroethylene, acetone and methanol baths followed by de-ionized (D.I.) water rinsing, was used for degreasing. Prior to deposition, the substrates were etched in 10 % HF solution for 4 minutes in order to remove oxides layers on the surface and then carefully rinsed in D.I. water.

In MOCVD growth, the precursors were thermally decomposed and reacted to deposit thin films on the substrate. Experimental variables that determine the resultant products were substrate temperature (T_s), reactor pressure (P_r), and source gas flow ratio ($R_{s/w}$) defined as Ar(H_2S)/Ar(W(CO)$_6$), all of which were optimized in order to obtain the desired thin film chemistry and microstructure. In the deposition strategy, each parameter was

successively varied with other variables fixed. For example, deposition was attempted by varying the substrate temperature, while both the reactor pressure and reactants flow ratio were fixed. The resultant thin films were characterized by various techniques described below.

C. CHARACTERIZATION OF THE WS$_2$ LAYERED THIN FILMS

C.1 CHARACTERIZATION PROCEDURES

Thin film crystal structure was routinely characterized by x-ray diffraction (XRD) in θ–2θ geometry using Cu-Kα radiation with a Phillips PW-1830 diffractometer.

Surface morphology was observed at various stages of thin film growth in a JEOL 5200 scanning electron microscopy (SEM). An atomic force microscope (AFM) (Digital Instruments, Nanoscope III) was also employed in order to characterize the thin film morphology at the early stage of deposition. AFM was operated in contact mode while keeping a constant tracking force in air.

Transmission electron microscopy (TEM) observation was made of plan-view samples using a Philips EM430 microscope operating at 200 kV. High resolution electron microscopy (HREM) observation of cross-sectional samples was made at 400 kV using a JEOL-4000EX microscope. Plan-view samples were prepared by procedures peeling off a thin film using a steel knife, putting the film to distilled water, and then collecting the fragments on copper grids. Cross-sectional samples were made by a sandwich method: gluing two pieces of materials face-to-face using epoxy, slicing the bulk to a plate of about 0.5 mm thickness, mechanically grinding the plate to about 100 μm thickness, and then thinning by ion milling.

Raman spectra were taken using the 632.8 nm line of a He-Ne laser at 17mW of power. The scattered radiation was analyzed using an 1800g/mm grating with an air cooled 1024 x 256 pixel array CCD detector. A spectrum resolution of 2.5cm^{-1} was obtained in 3 pixels (or < 1cm^{-1} per a pixel). All data were obtained under ambient conditions, but care was taken to ensure that no discernible laser damage took place in the film by repeating scans at different positions. All samples did not show any visible change even after prolonged periods of the laser irradiation at each position.

C.1 PREFERRED ORIENTATION OF WS$_2$ THIN FILM GROWTH

Deposition process was tuned by changing the experimental parameters (T_s, P_r and $R_{s/w}$) so as to obtain the desired chemistry and structure of WS$_2$ thin films. Shown in Fig. 4 is a series of x-ray diffraction spectra obtained from the thin films deposited by

varying the substrate temperatures (Ts) from 583K to 723K with other parameters fixed (P_r = 0.75 Pa and $R_{s/w}$ = 0.66). The deposition time was 10 minutes for each case. An XRD spectrum from $2H$-WS_2 single crystal is also included in Fig. 4 for comparison.
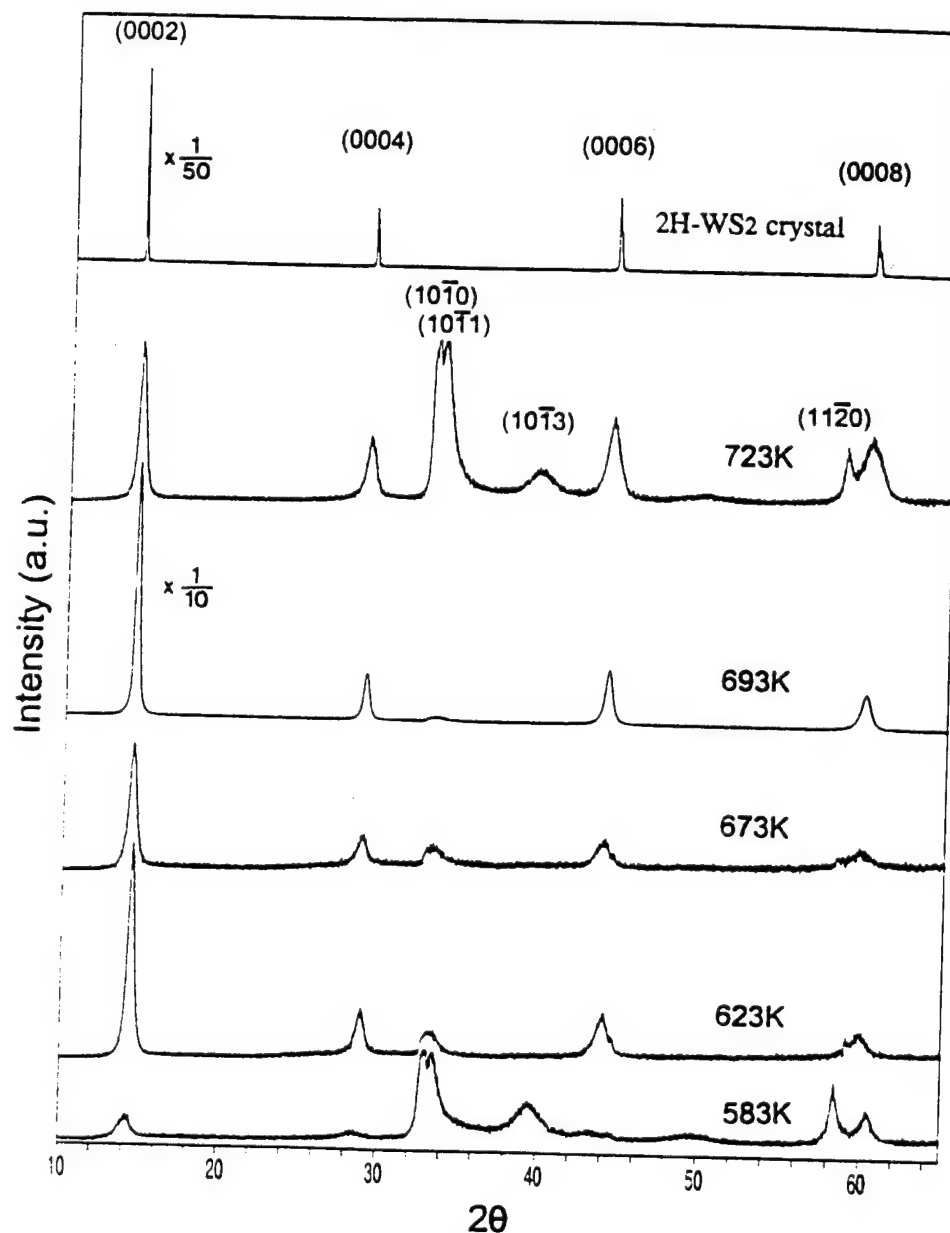

Fig.4   X-ray diffraction spectra of WS_2 single crystal and thin films prepared at various temperatures from 583K to 723K. The reactor pressure and source gas flow ratio were set at 0.75 Pa and 0.66, respectively. Sample thickness was approximately 200 nm for all cases.

-13-

The spectrum of the single crystal is characterized by a series of peaks consisting of (0002), (0004), (0006), and (0008) peaks, which correspond to the reflections from the basal planes of WS_2. Similar sets of diffraction peaks are observed in the MOCVD-grown WS_2 thin films. The appearance of these peaks implies that the thin film contains the crystallites with their basal planes parallel to the substrate. Hereafter, we denote such crystallites as c(=). As is evident in Fig. 4, there is a set of peaks consisting of $(10\bar{1}0)$, $(10\bar{1}1)$, $(10\bar{1}3)$ and $(11\bar{2}0)$ in the spectra of the thin films. These peaks originate from the crystallites with basal planes non-parallel to the substrate. We denote these crystallites as c(//). Based on XRD results, it is found that the deposition at around 693K ($P_r = 0.75$ Pa and $R_{S/W} = 0.66$) yields thin films with their basal planes most highly oriented parallel to the substrate; and the fraction of c(//) is minimized in the structure. The (0002) peak occurs at 14.37° in 2θ, which is nearly at the same value for the 2H-WS_2 single crystal. The full width at half maximum (FWHM) of the peak from the thin film is, however, considerably wider than that observed from the single crystal. As the structure becomes more mixed with c(//) crystallites, the FWHMs are further broadened, although the (0002) peak position is unchanged.

In order to evaluate the relative significance of the deposition parameters, T_s, P_r, and $R_{S/W}$, in relation to the degree of preferred orientation, a parameter, Σ, as defined below is introduced:

$$\Sigma = \frac{c(=)}{c(//)} = \frac{\dfrac{I_{(0002)}}{FWHM_{(0002)}}}{\dfrac{I_{(10\bar{1}0)}}{FWHM_{(10\bar{1}0)}} + \dfrac{I_{(10\bar{1}1)}}{FWHM_{(10\bar{1}1)}} + \dfrac{I_{(11\bar{2}0)}}{FWHM_{(11\bar{2}0)}} + \dfrac{I_{(10\bar{1}3)}}{FWHM_{(10\bar{1}3)}}}$$

In this equation, the parameter, Σ, characterizes the fraction of crystallites, c(=) and c(//), as measured by their peak intensities and FWHMs. The intensity, $I_{(0002)}$, represents the amount of c(=) present in the film, whereas the sum of the intensities for $(10\bar{1}0)$, $(10\bar{1}1)$, $(10\bar{1}3)$ and $(11\bar{2}0)$ peaks, or $I_{(10\bar{1}0)}+I_{(10\bar{1}1)}+I_{(11\bar{2}0)}+I_{(10\bar{1}3)}$, corresponds to the amount of c(//) crystallites present in the film. In the analysis, one way of expressing the relative fraction of the c(=) and c(//) crystallites in the thin film structure is to simply calculate the ratio for $I_{(0002)}/(I_{(10\bar{1}0)}+I_{(10\bar{1}1)}+I_{(11\bar{2}0)}+I_{(10\bar{1}3)})$. This does not, however, include any measure of the crystallinity of the thin films. In order to remedy this, each peak intensity was divided by its FWHM value, and was used as a corrected intensity. The equation defined above, therefore, contains information regarding the amount of crystallites present in the thin film, and their crystallinity.

Shown in Fig. 5 is a semi-log plot for various Σ versus T_s for different P_r and $R_{S/W}$ values. In this plot, large Σ values (>100) represent the conditions in which WS_2 thin films are formed with a high degree of orientation with basal planes parallel to the substrate. Obviously, if all the basal planes are grown parallel to the substrate, such as the case of single crystal WS_2, this quantity becomes infinite. For $\Sigma < 1.0$, thin films contain

a large fraction of basal planes grown non-parallel to the substrate. Although the value Σ does not represent the actual fraction of c(=) and c(//) in the film structure, this plot is found to be very useful in evaluating the effects of the experimental conditions on the structure of the deposited films.
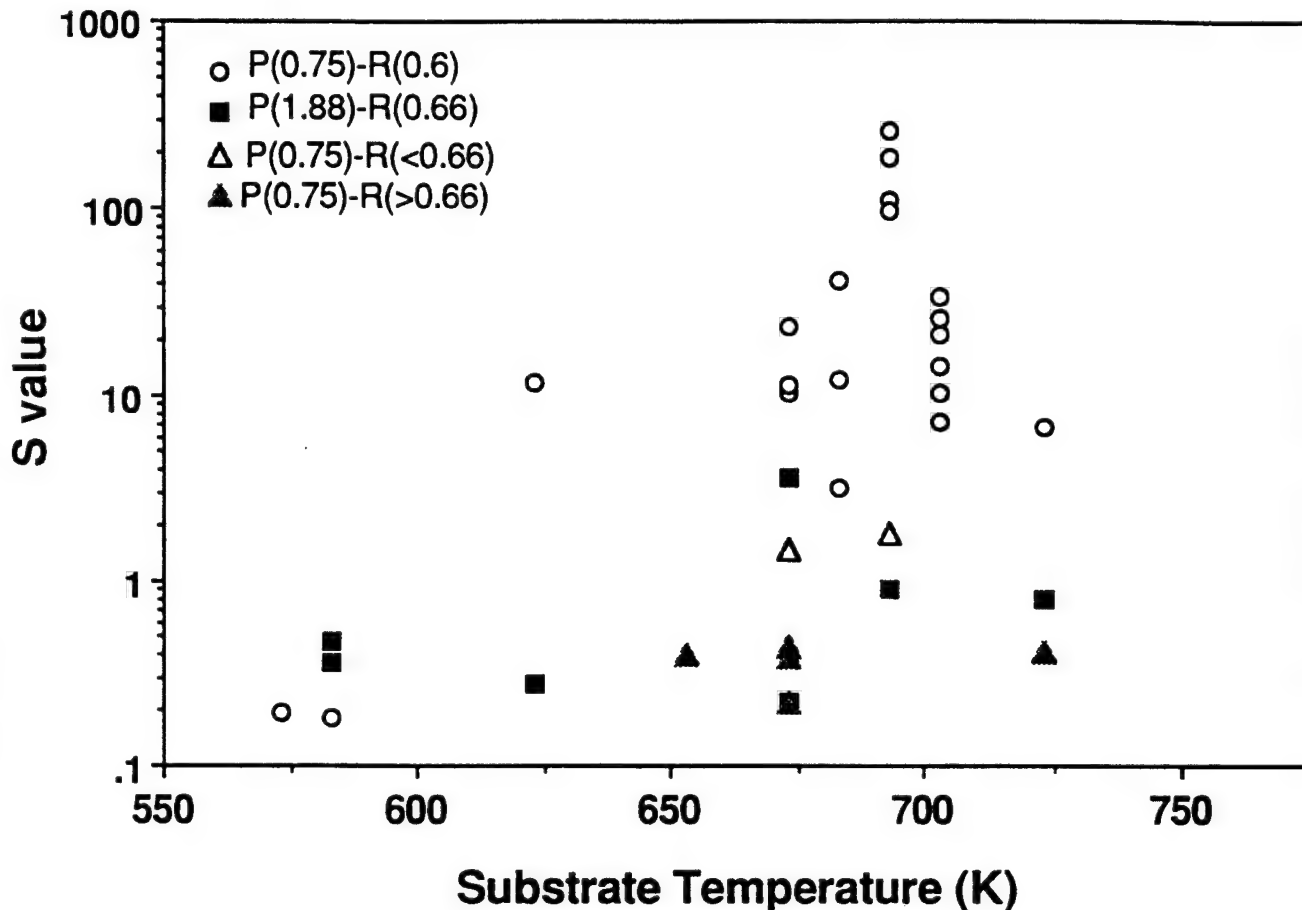
Fig. 5 Semi-log plot for Σ versus T_S for different P_r and $R_{S/W}$ values. Σ was determined by the equation described in the text. Legend in the figure, for example, o P(0.75)-R(0.6) means that the deposition was made by varying T_S with P_r=0.75 Pa and $R_{S/W}$ = 0.66 fixed.

The total thickness of WS_2 thin films was measured directly from the cross section of its cleavage plane by scanning electron microscopy. Average growth rates were determined by dividing the total thickness by the deposition time for each set of the deposition conditions. While the growth rates are found to be strongly dependent on the deposition conditions, it is generally noted that the conditions that yield Σ >100 exhibit relatively small growth rates, whereas higher growth rates are obtained for Σ values between 1 and

100. An average growth rate for the specimens showing highly preferred orientation, or $\Sigma > 100$, was on the order of 15 nm/min, whereas a range of growth rates between 20 and 35 nm/min is observed for conditions that yield $1 < \Sigma < 100$. For $\Sigma < 1$, the growth rate was reduced substantially, and was not accurately determined.

C.2 THIN FILM MICROSTRUCTURE

The microstructure of WS_2 films for which deposition conditions have yielded high Σ values (>100) were examined by TEM and HREM techniques.

Fig. 6(a) shows a plan-view TEM bright-field image in which a typical morphology of the WS_2 thin film is displayed. The deposition condition was $T_S= 693K$, $P_r = 0.75$ Pa and $R_{s/w} = 0.66$. The film consists of crystallites with bright contrast and some crystallites with dark or gray contrasts. The crystallites with dark contrast have a cigar shapes. The gray crystallites look like plate but their shapes are not quite regular. By tilting the sample, they can change into cigar-shaped dark crystallites and the dark crystallites can change into gray ones. This indicates both dark and gray crystallites are of a similar kind but their orientations are different within the film.

In order to determine crystallographic orientation of the WS_2 film, microdiffraction technique has been employed. Figure 6(b) is a micro-diffraction pattern with the [0001] zone axis taken from the region with bright contrast. The lattice parameter calculated from the diffraction pattern was 0.311nm, consistent with a_o of the 2H-WS_2 type crystal. Similar patterns were observed from many other areas. This indicates that the crystallites distributed in the bright contrast correspond to the c(=)-WS_2. The micro-diffraction pattern shown in Fig. 6(c) was taken from the region including both dark contrast and bright contrast area. In this pattern, a set of (0002), (0004), and (0006) are the diffraction spots from the area with dark contrast. An hexagonal pattern similar to one obtained from the area with bright contrast is superposed. A lattice parameter calculated from the set of (0002), (0004) and (0006) diffraction points was 1.221nm, which was consistent to c_o of the 2H-WS_2 single crystal. This result indicates that the c-axes of the acicular crystallites are perpendicular to the direction along its long side and parallel to one of the reciprocal directions $[10\bar{1}0]^*$ of the c(=)-WS_2 crystallites. The crystallites with gray contrast are responsible for the c(//)-WS_2.

The microstructure of the thin films was further characterized by cross-sectional HREM shown in Fig. 7. The incident electron beam was parallel to a <110> direction of the Si (100) substrate. Following an amorphous layer, WS_2 thin films were grown layer-by-layer with basal planes nearly parallel to the (100) plane of the Si substrate. This layered growth feature extended to more than 30 nm is clearly observed. The lattice image for WS_2 was further analyzed by a computer simulation. In this process, observed lattice images were electronically filtered to eliminate high frequency noises. A series of computer

simulations to generate lattice images were made by varying sample thickness and defocused conditions of the microscope as the input parameters. In Fig 8, an observed image of WS_2 lattice (a) and its filtered image (b) are compared with the best matched image simulation (c) with their atomic position shown in (d). Form these image simulations, the synthesized WS_2 possessed a $2H-WS_2$ polytype structure. An averaged spacing between the layers measured from the image was approximately 0.624 nm, which was consistent with the value obtained from X-ray diffraction analysis. This value is, however, slightly larger than the one known for $2H-WS_2$ single crystal (0.618 nm [8]). The inhomogeneous image contrast indicates that the thin film consists of multiple domains. It can be seen that uniform growth of the layers appears to be terminated by forming stacking faults and other types of defects, and the average domain size ranges from 3 to 5 nm.
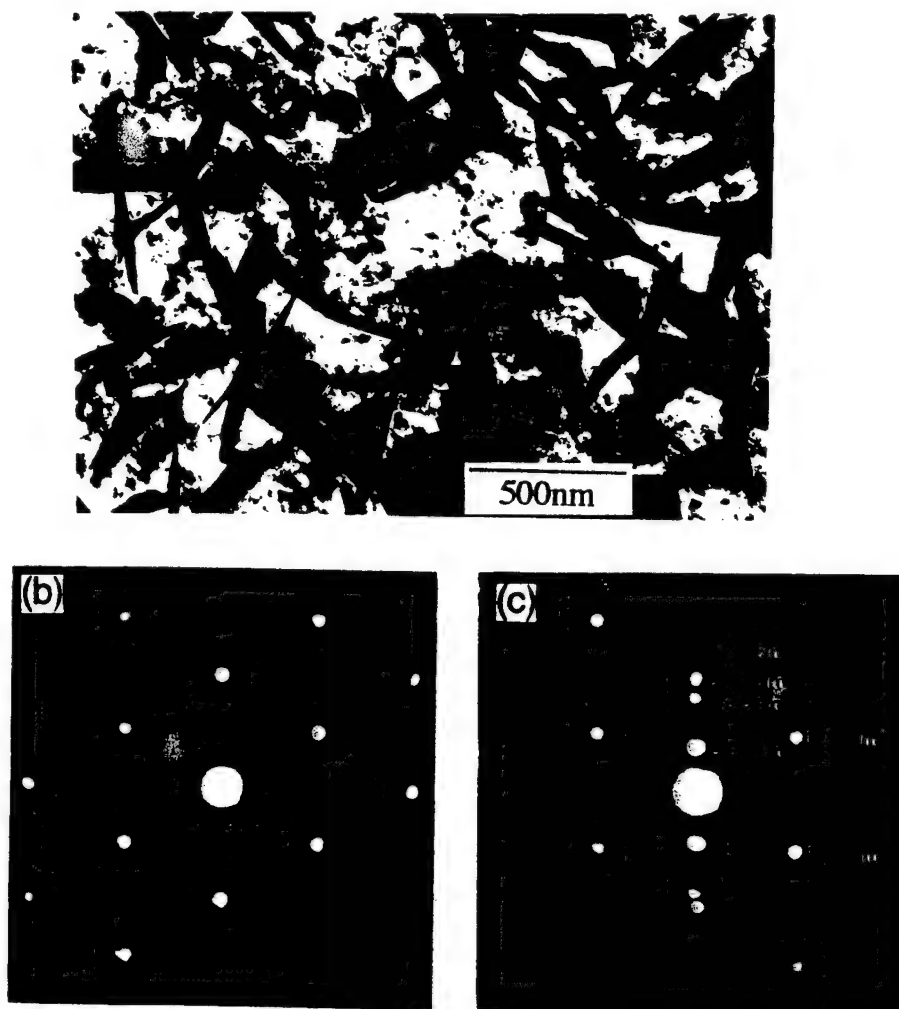
Fig. 6 (a) Plan-view TEM bright-field image of WS_2 thin film prepared at the deposition condition of T_S= 693K, P_r = 100 torr and $R_{s/w}$ = 0.66. (b) micro-diffraction pattern taken from the region with bright contrast, (c) micro-diffraction patterns taken from the region including both dark contrast and bright contrast.

Fig. 7 HREM image of the WS_2 / Si(100) interface. The incident electron beam was parallel to <110> direction of the Si (100) substrate.
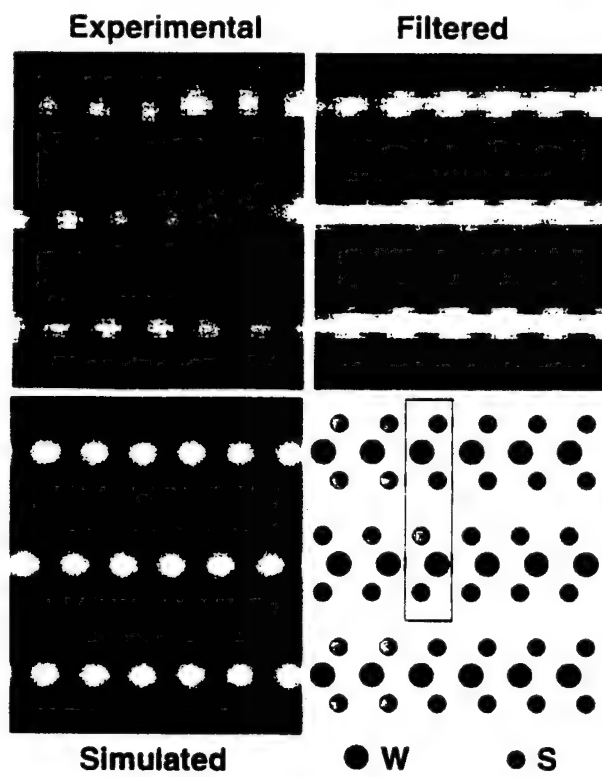
Fig. 8 Comparison between HREM lattice image and computer simulated lattice image.

As thickness increases, the layer structure becomes wavy, showing an increasing density of structural defects. In addition, the thin films are grown with their basal planes "less" parallel to the substrate. This type of growth continues to a thickness of ~30 nm, then several portions of the layers start to grow in different directions, i.e., growth with basal planes non-parallel to the substrate, as shown in Fig. 6. This image clearly shows one crystallite of thickness around 20 nm is developed with their c-planes nearly perpendicular to the substrate. Several other crystallites have grown with growth directions rotated by approximately 30°, 45° or 60°. These crystallites are responsible for $c(//)$ in the thin films. While these specific angles are obtained from the image, it may be related to preferred orientations for hexagonal lattice structure; details are currently under investigation.

Fig. 9 HREM cross sectional image of MOCVD-WS$_2$ thin film after 10 minutes deposition on Si(100).

C.3 SURFACE MORPHOLOGY

Cross-sectional HREM micrographs revealed that WS_2 thin films grew with van der Waals planes parallel to the substrate near the interface, and then cigar-shaped acicular crystallites developed as the thickness increased. The development of the acicular crystallites along with increasing film thickness were studied by looking at the change in surface morphology of the thin films. Several thin film specimens with different thicknesses were prepared by varying the deposition time. Surface morphology was investigated by atomic force microscopy (AFM) and scanning electron microscopy (SEM).

The surface morphology of a WS_2 thin film after 2.5 minutes deposition (thickness is about 30 nm) observed by AFM is shown in Fig. 10. Owing to the superior sensitivity for the depth resolution of AFM technique, surface morphology at the early stage of the growth is clearly identified. The specimen was prepared using the deposition condition of $T_S = 693K$, $P_r = 0.75$ Pa, $R_{S/W} = 0.66$, which yielded a high Σ value. AFM micrograph reveals that the surface consists of several triangular-shaped islands, which intersect to each other at angles of 60°. This morphology is related to a primitive hexagonal islands of WS_2 crystallites, nucleating and growing on top of the preceding layers in a layer-by-layer fashion. The height of the triangular islands was estimated to be approximately 1.3 nm from the micrograph. This value is nearly a twice the WS_2 layer thickness (0.618 nm for each layer), indicating the formation of a $2H$-WS_2 structure. A closer look at the micrograph reveals that several corners of the triangular islands are curled up from the surface. This may be the origin of $c(//)$ crystallites in the thin films.
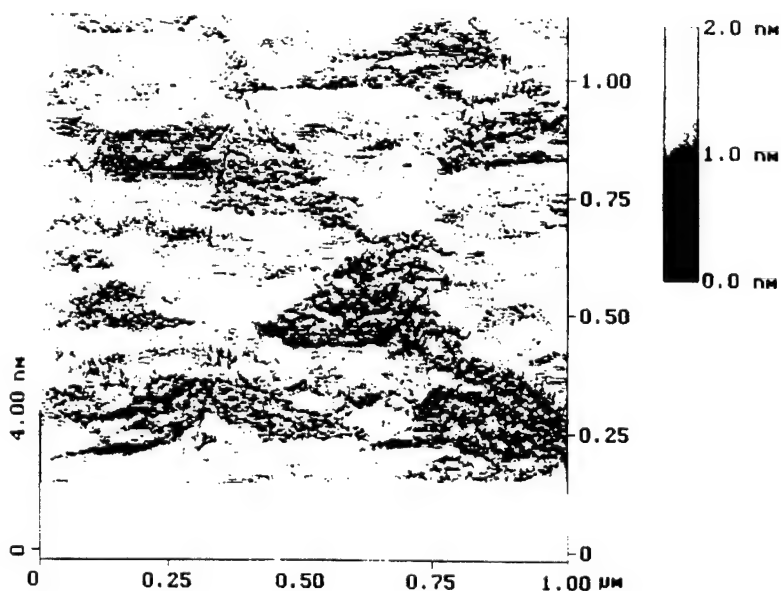
Fig. 10 Surface morphology observed by AFM

By continuing to increase the deposition time to prepare thicker specimens, surface morphology was further characterized by SEM. Fig 11 (a), (b), and (c) show a series of SEM micrographs observed from thin film surfaces after deposition times of 5, 10 and 15 minutes, respectively. Average thicknesses were 65 nm, 170 nm and 350 nm, respectively, although thickness varies considerably from position to position as the deposition time increases. Micrograph (a) shows a number of needle-like crystals, indicating the beginning of acicular crystallites developed from the $c(=)$-WS_2. The directions of the needle-like crystals are not random, but occur at angles of 30°, 60° and 90° with each other. As the thickness increases, acicular crystals with length ranging from 100 nm to 400 nm develop (Fig. 11(b)). The appearance of these crystallites is consistent with the plan-view micrograph shown in Fig. 6(a). With further increases of thickness, the density of the acicular crystallites increases significantly, but the size remain nearly the same (Fig. 11(c)).
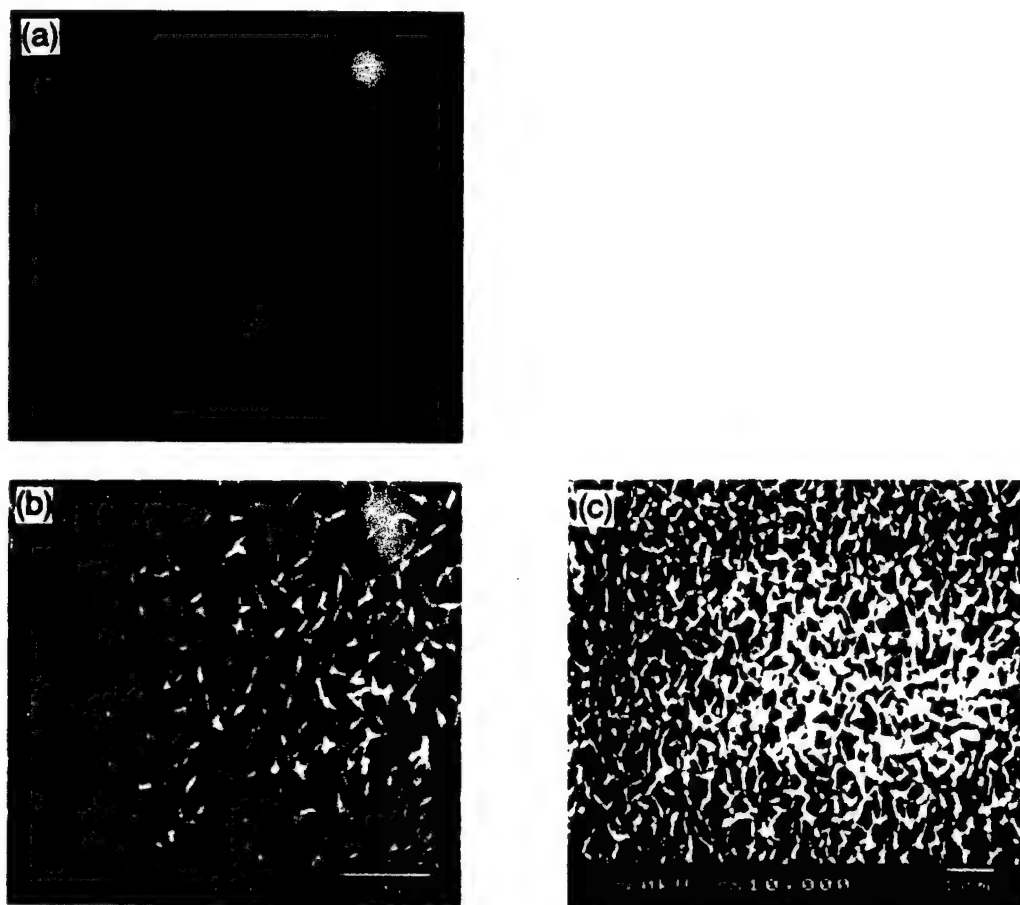
Fig.11 A series of SEM micrographs observed from thin film surfaces after the deposition times of (a) 5 minutes (corresponding average thickness was 65 nm), (b) 10 minutes (170 nm), and (c) 15 minutes (350 nm), respectively. Deposition condition was $P_r = 0.75$ Pa, $T_S = 693K$, $R_{S/W} = 0.66$.

C.4 CRYSTALLINITY AND STATE OF STRESS IN WS$_2$ THIN FILMS

Raman Scattering is known to be sensitive to small changes that occur in the lattice symmetry of a crystal, therefore, it has been used as a sensitive structure probe in particular to study the defects in solids [9]. Since the sensitivity of the Raman effect in solids is primarily due to the movement of an atom pair which induces a corresponding movement in all the nearest neighbors, any structural change associated with the different preferred orientations may influence the Raman scattering phenomena. We have applied the Raman spectroscopy to evaluate the state of stress induced by the preferred orientations, c(=) and c(//). Results are compared with those obtained from a single crystal WS$_2$ specimen, and further correlated to the atomic structure of thin films observed by high resolution electron microscopy (HREM).

Three sets of specimens (a) 2H-WS$_2$ single crystal, (b) 2H-WS$_2$ thin film with high Σ value (or high c(=)/c(//) ratio), and (c) 2H-WS$_2$ thin film with low Σ value (or low c(=)/c(//) ratio), were examined by the Raman spectroscopy, and their results are shown in Fig. 12. The Raman spectrum obtained from a WS$_2$ powder specimen is also included for comparison. In all cases, the spectrum is characterized by two major peaks along with a number of small peaks distributed throughout the spectral range in good agreement with those reported previously [10]. As the long wavelength vibrational modes for 2H-WS$_2$ have been discussed in detail by many workers, the first major peak at around 350 cm^{-1} is assigned as the E$_{2g}$ mode for the motion of W+S atoms in the x-y layered plane, and the second peak at around 420 cm^{-1} is the A$_{1g}$ mode for the motion of two S atoms along the z-axis of the unit cell . The small peaks appearing between 100 cm^{-1} and 600 cm^{-1} correspond to the second order Raman (SOR) peaks which arise from phonon couplings with a non-zero momentum [11]. These SOR bands can be seen more clearly in a spectrum in which the scale has been expanded by a factor of 5, and are also shown in Fig. 12.

During the course of this work, we have noticed that the Raman peak at around 420 cm^{-1} observed from the thin film specimens is non-symmetric, and considerably broader than that observed from the single crystal specimen. The peak consists of two components, one appearing consistently at around 421 cm^{-1}, and the other appearing as a shoulder at lower wave numbers as indicated by an arrow in Fig. 13. Using a curve fitting technique, the relative peak area for the shoulder peak to the peak centered around 421 cm^{-1} was computed for every thin film specimen examined in the present experiment. They are plotted in Fig. 14 as a function of Σ value. The relative concentration of the shoulder peak was increased when the fraction of c(//) became larger. While the powder WS$_2$ specimen exhibits a small shoulder peak in the same way as the thin film specimen does, the single crystal WS$_2$ does not show such a peak. These facts imply that the shoulder component associated with the A$_{1g}$ mode may be induced by some kind of structural disordering in the thin films. As will be seen next, the origin of this shoulder peak is related to the forbidden SOR effect which is attributed to disorder-activated zone boundary phonons, as

was originally suggested by Cingolani et al. during their study of zone boundary phonon interactions in GaS [11].
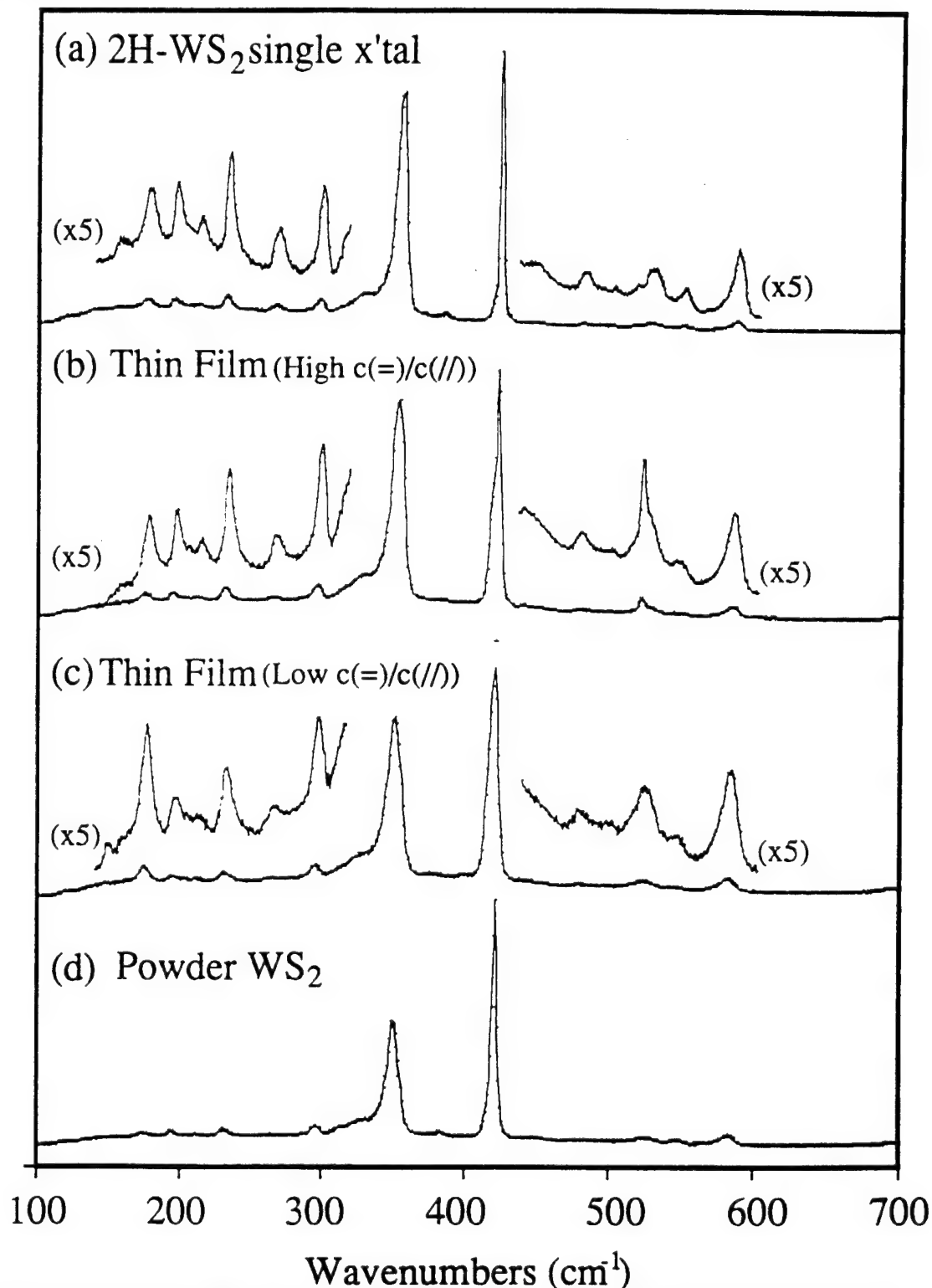
Fig.12 Raman spectra taken from (a) 2H-WS$_2$ single crystal, (b) 2H-WS$_2$ thin film with high Σ value (high $(=)/c(//)$ ratio), and (c) 2H-WS$_2$ thin film with Σ value (low $c(=)/c(//)$ ratio).
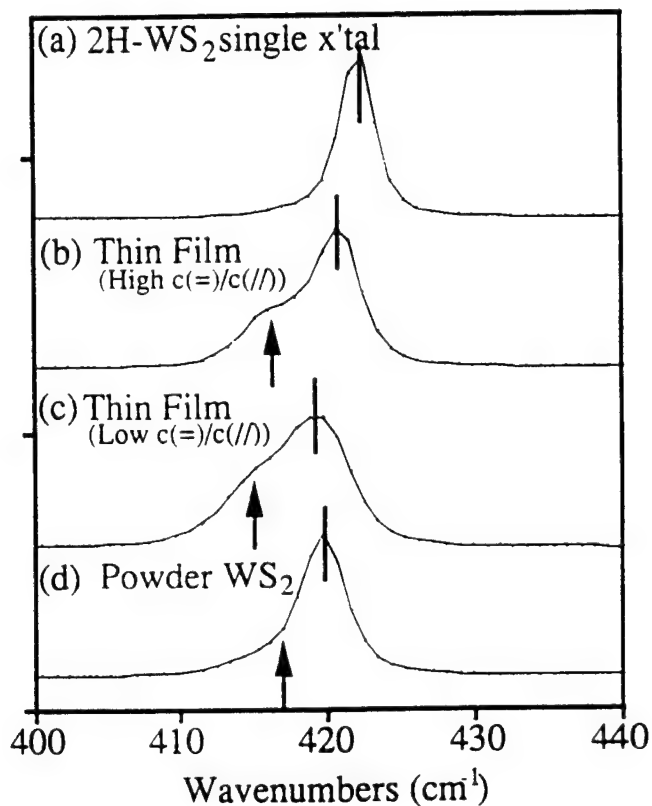
Fig. 13 Expanded Raman spectra around 420cm^{-1} observed from (a) 2H-WS$_2$ single
crystal, (b) 2H-WS$_2$ thin film with high c(=)/c(//) ratio, and (c) 2H-WS$_2$ thin film
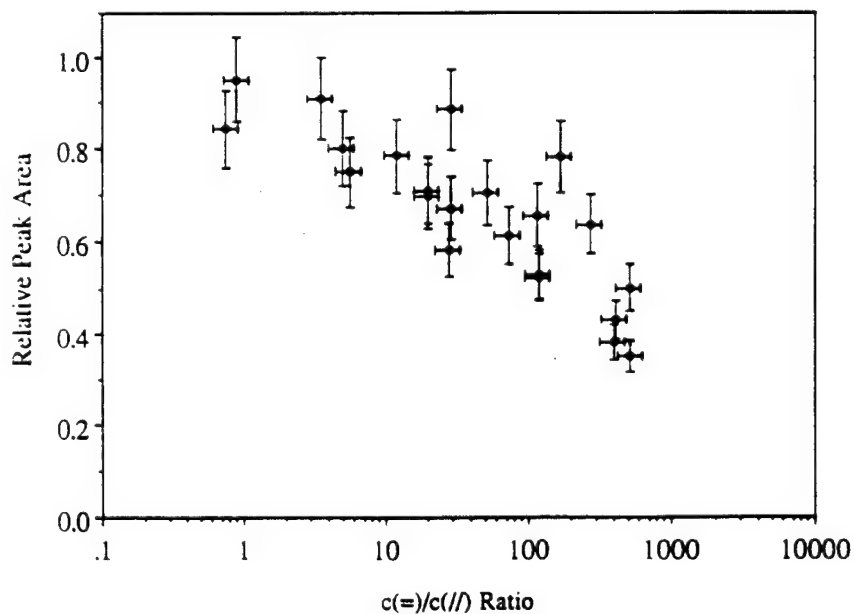with low Σ value (c(=)/c(//) ratio).

Fig. 14 Variation of the relative peak area for the shoulder peak to the peak centered
around 421cm^{-1} as a function of parameter, Σ (c(=)/c(//)).

In order to study the evolution of the shoulder peak as seen in Fig. 13, Raman spectra (a), (b) and (c) shown in Fig. 4 were characterized in detail by assigning SOR bands in the manner that Sourisseau et al. did for the 2H-WS$_2$ single crystal [12]. In their analysis, the measurable SOR peaks were assigned to combinations of sum or difference bands involving phonons at the K point of the Brillouin zone, coupled to the longitudinal acoustic phonon mode, LA(K). In Table II, Raman band wavenumbers (cm^{-1}) and assignment of the bands as reported by Sourisseau et al. along with our experiments are tabulated.

Table II. Assignment of the Raman bands from (a) 2H-WS$_2$ single crystal, (b) WS$_2$ thin film with high Σ value, and (c). WS$_2$ thin film with low Σ value.

| Raman band | | Assignments[16] | | Our measurements | | |
| | | 1st order | 2nd order | (a)WS$_2$ x'tal | (b)Thin film | (c)Thin film |
(cm^{-1})	int.	(at Γ point)	(at K point)	(cm^{-1}) int.	(cm^{-1}) int.	(cm^{-1}) int.
27.4		$E_{2g}^2(\Gamma)$		N/A	N/A	N/A
139	vw		$E_{1g}(K) - LA(K)$	139.8 vw	138.0 vw	137.0 vw
178	w		$E_{2g}^1(K) - LA(K)$	176.2 mw	174.3 mw	174.3 mw
198	vw		$B_{2g}(K) - LA(K)$	195.3 mw	195.3 mw	195.3 mw
233	m		$A_{1g}(K) - LA(K)$	232.3 m	231.4 m	230.4 m
325	ms		$2LA(K) - E_{2g}^2(K)$	329.1 m	328.1 m	326.3 m
352	ms		$2 \times LA(K)$	350.4$^+$ ms	349.0$^+$ ms	346.0$^+$ ms
356	s	$E_{2g}^1(\Gamma)$		355.1 s	353.3 s	350.5 s
384	vw		$2LA(K) + E_{2g}^2(K)$	383.8 vw	378.3 vw	374.6 vw
416	w		$LA(K) + TA(K)$	not seen	416.1* m	415.4* ms
421	s	$A_{1g}(\Gamma)$		422.5 s	420.7 s	419.8 s
480	w		$E_{1g}(K) + LA(K)$	481.1 w	478.3 w	478.3 w
523	m		$E_{2g}^1(K) + LA(K)$	528.2 w	528.2 w	521.9 w
544	ms		$B_{2g}(K) + LA(K)$	549.8 w	544.4 w	546.2 w
584	ms		$A_{1g}(K) + LA(K)$	586.6 w	583.9 w	582.1 w

Note: vw, w, m, ms, and s mean very weak, weak, medium, medium strong, and strong, respectively. $^+$ and * were estimated from curve fitting.

Simply comparing these data, our measured values for (a) WS$_2$ single crystal were in agreement with those reported within the wavenumbers of $\pm$ 2cm^{-1}. Raman band wavenumbers observed from the thin WS$_2$ film specimens, (b) and (c), were systematically shifted to the lower wavenumbers. Larger shifts were observed as the thin film contained more c(//) crystallites in the film structure. The analysis suggests that the shoulder peak can be assigned to two-phonon coupling originating from LA and transverse acoustic (TA) modes at the K point in the Brillouin zone of the WS$_2$ lattice. This mode was also seen in the powder WS$_2$ specimen, but not observed in the single crystal WS$_2$ specimen. These facts indicate that the LA+TA phonon coupling is forbidden under that perfect WS$_2$ lattice condition (as was observed in the single crystal), but structure disordering seems to activate the LA+TA mode in thin films. Evolution and such large enhancement of the LA+TA mode in WS$_2$ are reported for the first time.

The evolution of the detailed microstructure of the thin WS$_2$ films was previously shown in Fig. 9. Here another cross-section image obtained from a specimen with c(=)/c(//) value around 100 is shown in Fig. 15, where some portions of the van der Waals layers became non-parallel to the interface (c(//)) with increased thickness.
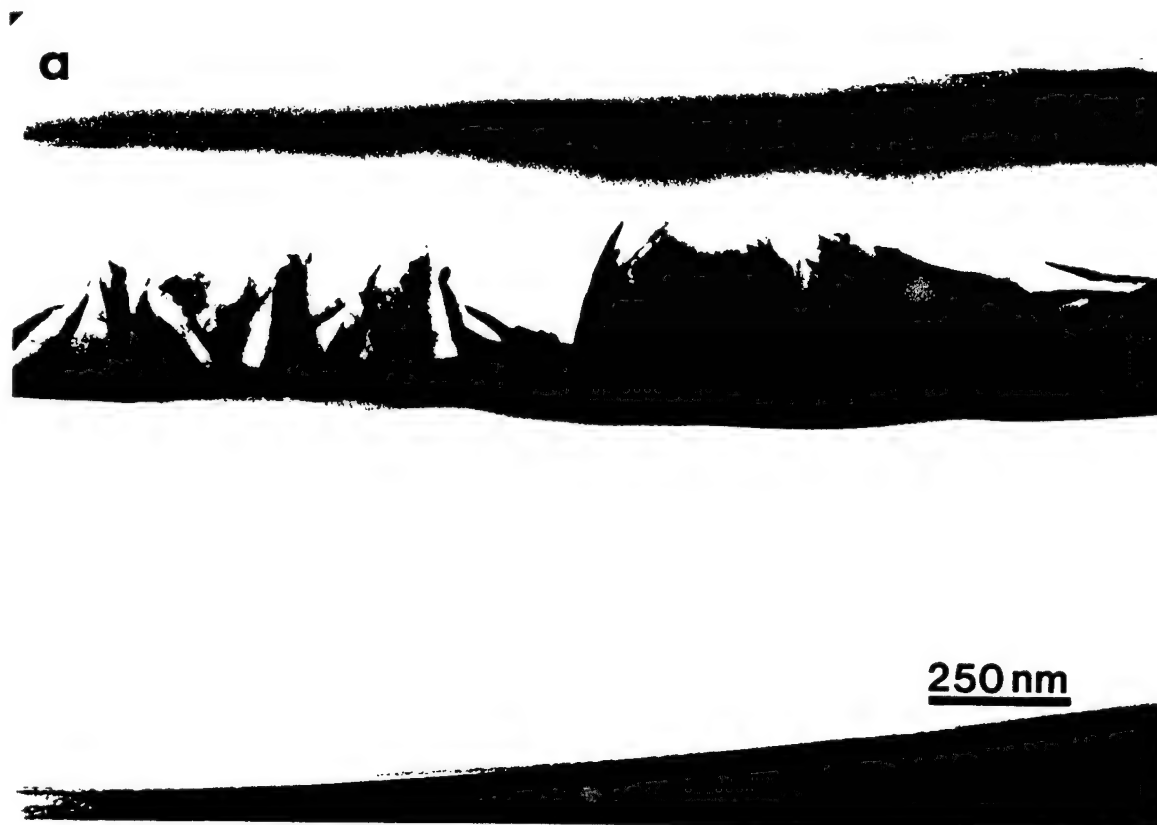

Fig. 15. Cross section high resolution electron microscopy image obtained from WS$_2$ thin film specimen with $\Sigma \approx 100$.

A close look at the micrograph reveals that transition from c(=) to c(//) occurs smoothly in the WS_2 layers, showing curvatures in the lattice image as seen in Fig. 16. Although the curvatures shown here are rarely seen, there are reports showing similar effects in some form of carbon and in minerals [13]. The ability of WS_2 to bend and the occurrence of localized curvature may contribute to the phonon coupling process. As shown in the micrographs, the basal orientation, c(=), dominates near the interface, however, local variations or disturbances of growth create regions of transition to c(//), where the lattice is subjected to a compressive stress on one side, and a tensile stress on the opposite site of the layers. One possible interpretation is that such disorder in the structure induced by the change from c(=) to c(//) may result in the breaking of the symmetry selection rules for Raman scattering, thus contributing to the spectra by loosening the forbidden conditions for phonon coupling at the different high symmetry of point of the Brillouin zone. In layered compounds like WS_2, acoustic branches are of particular interest, because they yield a direct measure of the interlayer and intralayer interactions. Cebula et al. [14] have previously reported limited measurements of the LA branch along the axis perpendicular to the plane of muscovite and hydrobiotite layered silicates. At this point, our interpretation is highly speculative in terms of mechanism, and the details must be worked out to reveal the effect of microstructure on the evolution of the 416 cm^{-1} SOR peak in the Raman spectra. Nevertheless the present finding suggests the importance of the microstructure on the enhanced second order Raman activity in the layered materials.

Fig. 16. HREM image the transition region from c(=) to c(//) in the specimen shown in Fig. 15.

C.5 WS$_2$ THIN FILM GROWTH PROCESS

The relative significance of various deposition parameters on the preferred orientation during the growth of WS$_2$ thin films has been studied carefully. Examining all the experimental results described in the previous sections, it is evident that the microstructure for MOCVD-grown WS$_2$ thin films is generally characterized by the formation of c(=) crystallites for the first few hundred Å, followed by a preferential growth of c(//) crystallites co-mixed with the c(=). Nowhere on the cross-sectional HREM micrograph has it been possible to observe the c(//) growing directly from the interface. They always appear to originate from the c(=), which implies that the nucleation and growth of crystallites having parallel orientation are initially favored since the basal plane is the lowest energy plane. A similar growth mode has been reported for MoS$_2$ thin films prepared by RF sputtering [15], and chemical vapor deposition technique[16]. Regula et al. have also observed nearly identical microstructure of WS2 thin films fabricated by RF sputtering [17].

A growth mode of MOCVD-WS$_2$ is schematically illustrated in Fig. 17.
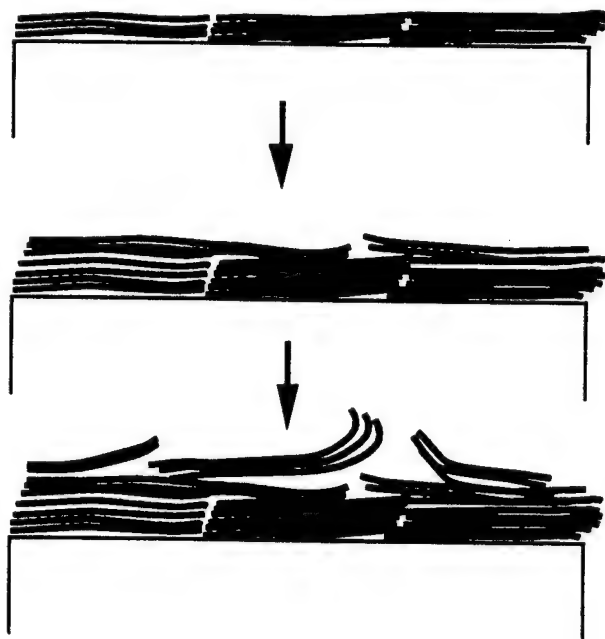
Fig. 17 Schematically illustrated cross-sectional morphology of MOCVD grown WS$_2$ thin film.

As the growth proceeds, when geometrical surface irregularities or stacking faults are induced, some crystallites with their reactive edge exposed to the gas-solid interface kinetically facilitate the preferred growth of WS_2 in directions non-parallel to the substrate surface. The orientation and anisotropic shape of the acicular crystallites indicates that WS_2 crystallites grow faster in the edge directions than in the basal direction. This is consistent with the fact that much higher growth rates for conditions that yielded low S values (higher degree of the formation of $c(//)$) were observed. Growth in the edge direction along the substrate surface appears to be somewhat impeded by the nucleation of the acicular islands. This growth pattern seems to be reasonable from a chemical viewpoint, since the edge surfaces of WS_2 are more reactive than the basal plane surfaces. Furthermore, lamellar type edge growth is favored from the standpoint of diffusion; since S and W planes are exposed, a mobile adatom on an edge surface can readily diffuse and attach onto a proper site. On the other hand, growth in the basal direction requires the sequential addition of an appropriate adatom species, which is a kinetically slower process. As for subsequent growth of AlN on top of this thin film material, the morphology of WS_2 plays a significant role, which will be mentioned next.

D.   DEVELOPMENT OF THE PROCESS TO DEPOSIT AlN THIN FILM ON WS_2 SUBSTRATE MATERIALS

D.1 DEPOSITION STRATEGY

Deposition of AlN thin films has been the subject of numerous investigations over the past years. Many techniques [18-25], including conventional chemical vapor deposition (CVD), metalorganic surface chemicals adsorption deposition (MOSCAD), laser induced chemical vapor deposition (LCVD), plasma chemical vapor deposition (PCVD), reactive molecular beam epitaxy (MBE), have been utilized.

In the present study, a technique called Atomic Layer Growth (ALG) for the synthesis of AlN thin films using novel precursors was adopted [26]. ALG uses self-limiting heterogeneous reactions at the substrate surface to form a film one atomic layer at a time. The fundamental concept of ALG is to limit the film formation mechanisms to heterogeneous reactions involving adsorbed species. Using this technique, one precursor (Group III) reacts with the surface in a self-limiting manner, i.e., one or less monolayers of the adsorbate is formed per deposition cycle. In the second step, the other precursor (Group V) then reacts in a facile, site-selective manner with the adsorbate of the first precursor to from the desired film. This process leads to an ordered nucleation and growth process in which highly ordered crystalline or epitaxial films can be grown. By utilizing nucleation and growth strategies that promote an ordered, site-selective growth mechanism, high temperatures for enhancing surface mobility are not required. The second step is what gives ALG its larger advantage over MBE techniques which lack a reactive nitrogen source that can be produced efficiently in particular for nitride formation. Coupling the ALG

technique with the use of novel amine-alane precursors can offer an exciting possibility for the thin film growth at low temperatures, with high purity and relatively fast deposition rate. In Fig. 18, sequential steps involved in ALG process are schematically illustrated.

"Atomic Layer Growth (ALG)" of AlN Thin Films

Dimethylethyl Amine-Alane

Ammonia

NH$_3$

Step-I

T= 693K

Step-II

T= 693K

Uptake   T= 693K

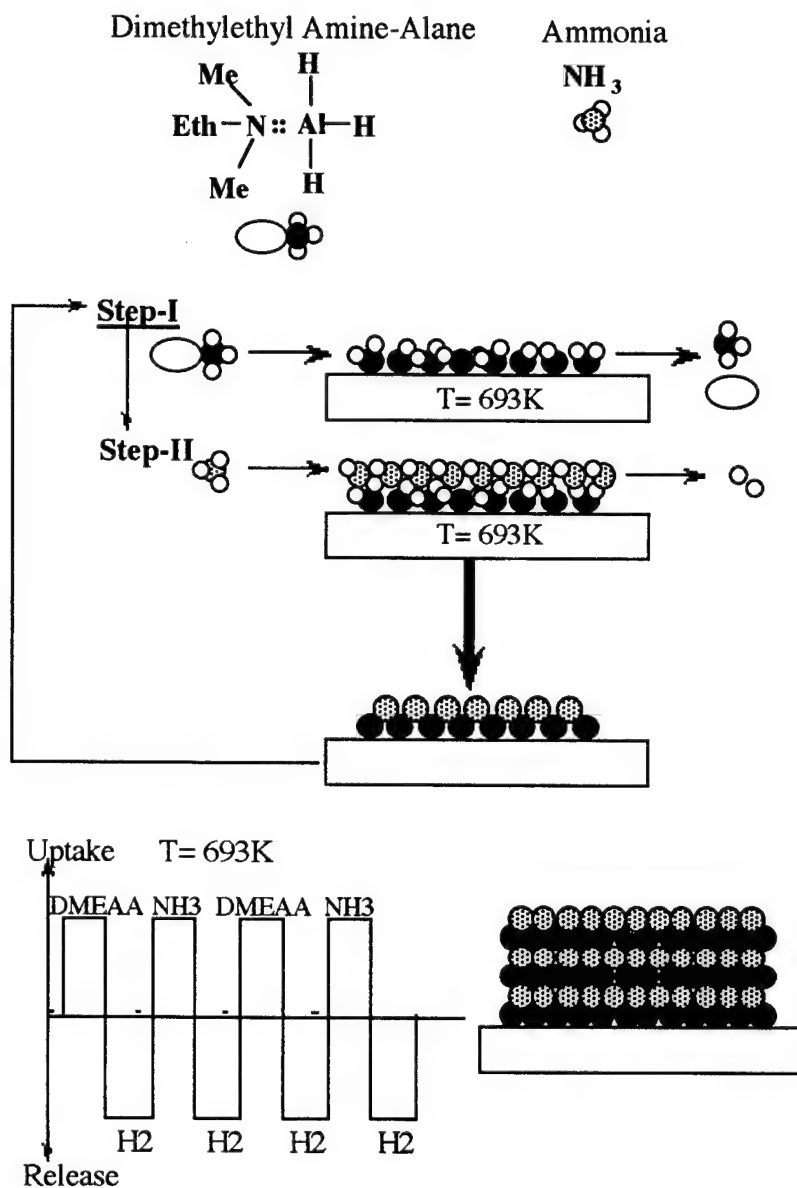DMEAA NH3 DMEAA NH3

H2   H2   H2   H2

Release

Fig. 18 Sequential steps involved in ALG process.

D.2 EXPERIMENTAL PROCEDURE

An ALG process for the deposition of AlN thin films as illustrated in Fig. 18. In this process, source gasses are alternatively introduced to the substrate surface by switching gals flow in a sequential manner, or using a rotating substrate under the low of separate gas stream. We have employed the first configuration, where a flush step of an inert gas is included between each reactant step in the sequence cycle to prevent gas-phase reactions. One cycle consists of four steps: i) a pulse of DMEAA for t_1 seconds, ii) a flush of pure carrier gas for t_2 seconds, iii) a pulse of NH_3 for t_3 seconds, and finally iv) a flush of pure carrier gas for t_4 seconds. An ALG process sequence is noted by the step duration as referred as a t_1-t_2-t_3-t_4 process. A typical sequence for the AlN thin film deposition was 4-5-4-5 process, where it consists of a 4 seconds DMEAA flow at a pressure of 4.93mtorr, a 5 seconds hydrogen flush, a 4 seconds ammonia flow in a pressure 2.5torr, then a 5 seconds hydrogen flush. The total flow of hydrogen to the reactor using as a carrier and flushing gas was 6 slm.

Deposition was carried out in a Crystal Specialities Inc. 425 MOCVD reactor equipped with a gas mixing manifold and three-say flush valves. In this apparatus, specially designed gas-mixing manifold enables for abrupt switching of the gas composition which is essential for the ALG process. A schematic diagram of the system is shown in Fig. 19.
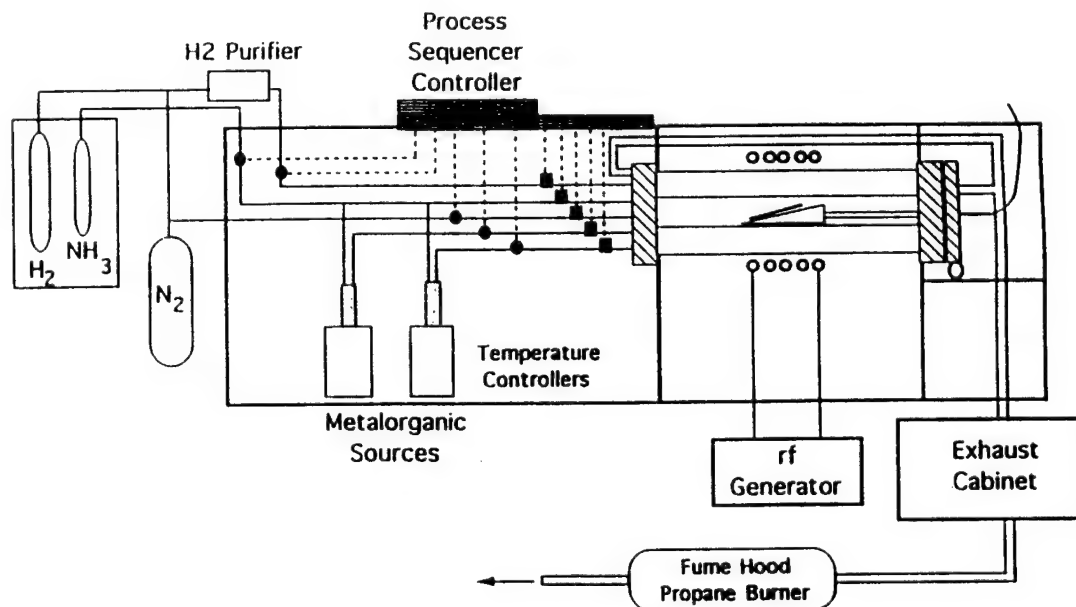

Fig. 19 Crystal Specialtilies Inc (CSI) 425 horizontal-style metalorganic chemical vapor deposition reactor.

D.3 AlN THIN FILM GROWTH BY ALG

D.3.1 AlN THIN FILMS ON WS$_2$ SINGLE CRYSTALS

Development of the ALG process for AlN deposition was accomplished in several sets of growth experiments. The goals of these studies were to first identify a parameter space where AlN thin films would be deposited and to improve the flow conditions. Previously we demonstrated the AlN growth on Si(100), Si(111) and Al$_2$O$_3$(0001) using identical precursors at temperature regime of $613\pm40°K$. We adopted similar conditions as the starting parameters, however, it was found that the process conditions for AlN deposition over WS$_2$ were quite different. From the series of experiments, the deposition procedure for the AlN growth on WS$_2$ was established as 4-5-4-5 sequences at 723°K with the reactor pressure ranging from 25 to 100 torr.

Figure 20 shows X-ray diffraction result obtained from AlN thin films deposited onto a single crystal WS$_2$ (0001) plane. The peak at $2\theta = 36.00°$ is due to diffraction from the AlN (002) plane. This fact also reveals that the AlN is preferably oriented in a direction parallel to the WS$_2$ (0001) plane and AlN thin film on WS$_2$ substrate had almost no strain since the peak displayed almost no shift from the correct position of Bragg's angle of 36.02°. The crystallinity of AlN films is also considerably good based on the value from the FWHM of (002) peak though the directional orientation can not be determined. In addition, AlN deposition was attempted on an Al$_2$O$_3$ substrate oriented with its surface along the basal plane of the crystal in order to compare the effects on the interface resulting from the different lattice mismatch at the same deposition conditions as the WS$_2$ substrate.

Figure 21 shows that AlN (001) plane has its preferred orientation along the basal plane of the Al$_2$O$_3$, (0001) plane. However, the peak at $2\theta = 35.89$ indicates that AlN thin film on Al$_2$O$_3$ substrate has experienced a larger stress than that the films deposited on the WS$_2$ substrate, based on the peak shift from the right position ($2\theta = 36.02$) of AlN in JCPD data file. The measurement of Poisson's ratio from the change of lattice constant by the stress after deposition indicated that AlN on WS$_2$ substrate had a much smaller change of lattice constant than that on Al$_2$O$_3$, so that $\Delta a_{ws2} = 0.27\Delta a_{Al2O3}$. In addition, the AlN crystals size of on WS$_2$ substrate displayed nearly the same size as those on the Al$_2$O$_3$ substrates which has a larger lattice constant than WS$_2$ as can be judged from the FWHM in X-RD peaks. The good lattice match between AlN and WS$_2$ substrate resulted in deposition of AlN thin films with good crystallinity as expected.
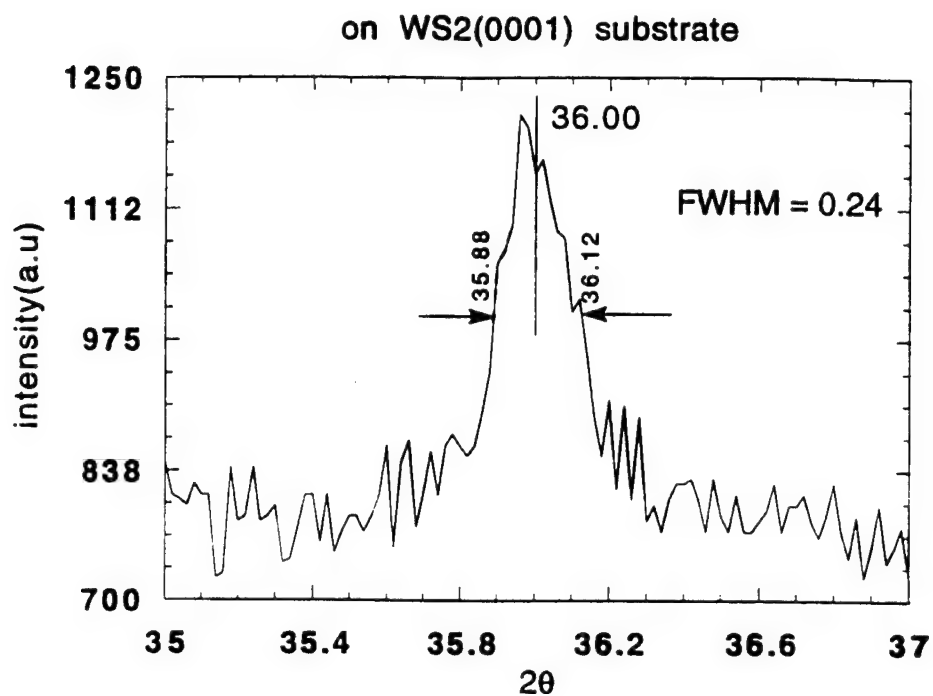
on WS2(0001) substrate

Fig. 20   XRD of AlN deposited on $WS_2(0001)$ single crystal surface

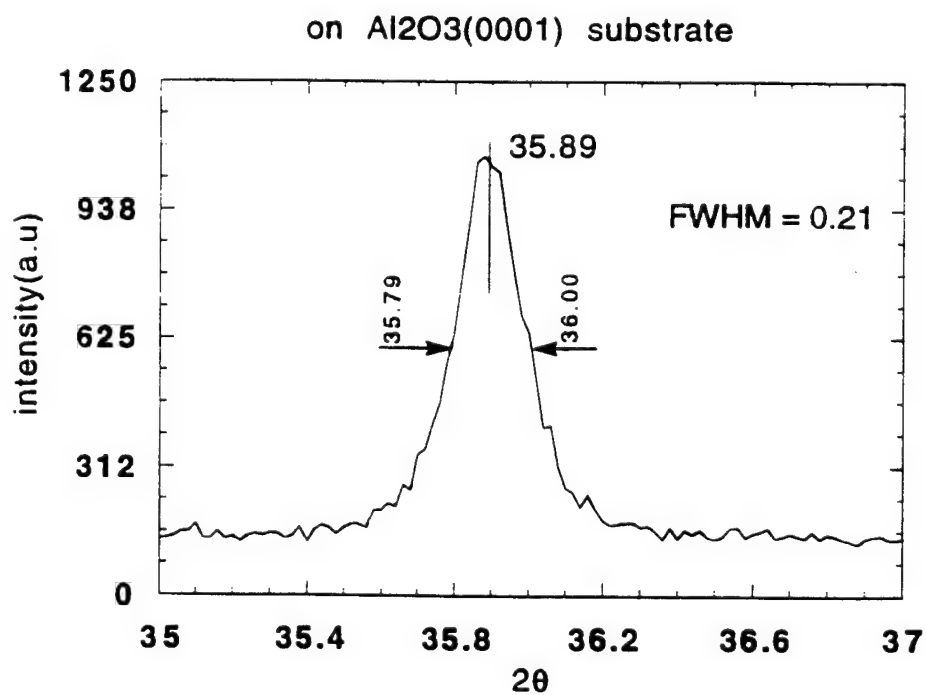## on Al2O3(0001) substrate

Fig. 21   XRD of AlN deposited on Al_2O_3 (0001) single crystal surface

D.3.2   AlN THIN FILMS ON WS$_2$ THIN FILM SUBSTRATES

Deposition of AlN thin films on typical WS$_2$ thin film ($\Sigma \approx 100$) substrate is presented first. X-ray diffraction spectrum is shown in Fig. 22. Thickness of the AlN layers was not accurately measured, however, the estimated thickness based on the deposition time was in the order of several hundred Å. Appearance of a series of WS$_2$ peaks, consisting of (0002), (0004), (0006), and (0008), indicates that the WS$_2$ thin film is oriented with the basal plane parallel to the substrate, however, a small fraction of non-parallel component exists. An AlN(0002) diffraction peak was detected at 2θ= 36.053° with the full-width-half-maximum (FWHM) of approximately xx°. Subset in Fig. 22 is the region corresponding to the AlN(0002) reflection peak. The presence of only one AlN diffraction peak in data indicated that AlN thin film has grown with the AlN{0001} planes aligned parallel to the substrate plane.
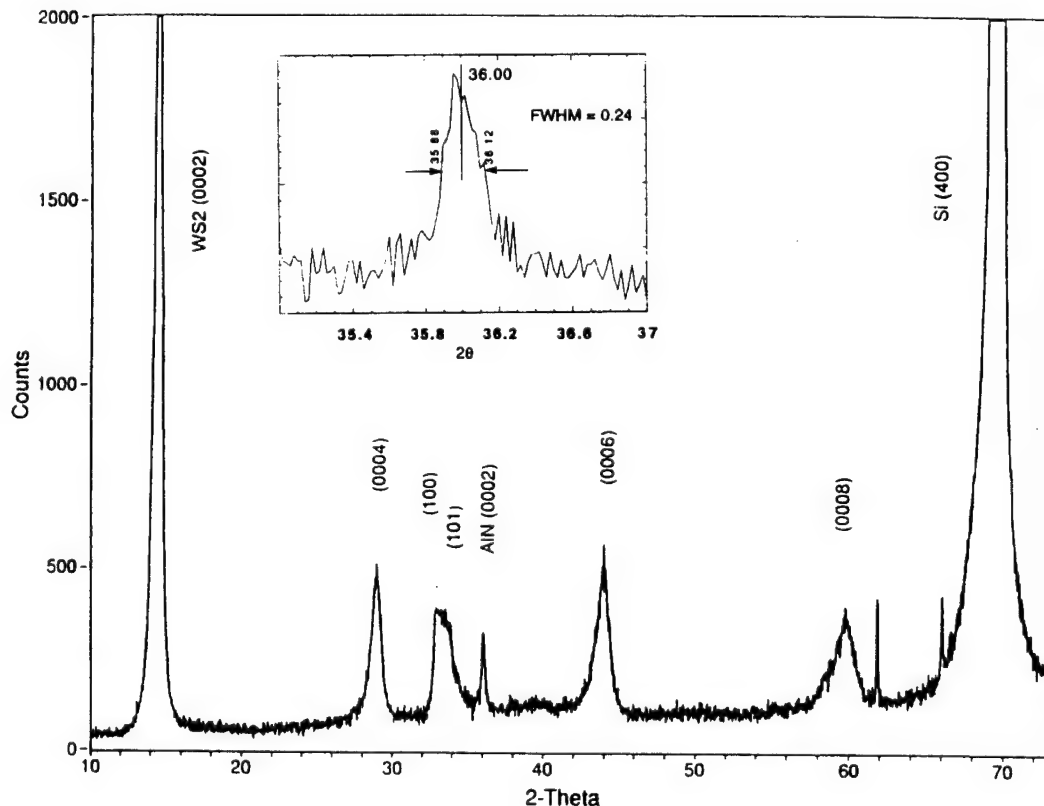

Fig. 22   XRD of AlN deposited on WS$_2$ thin films

Auger electron spectroscopy (AES) and X-ray photoelectron spectroscopy (XPS) were used to examined the chemical composition of the AlN films. Their spectra are shown in Fig 23 and Fig 24 for AES and XPS analyses, respectively. While both spectra obtained from the "as-received" specimen show substantial amount of oxygen, indicating surface

was oxidized by exposure to the ambient atmosphere, corresponding binding energies for N and Al were consistent to AlN.
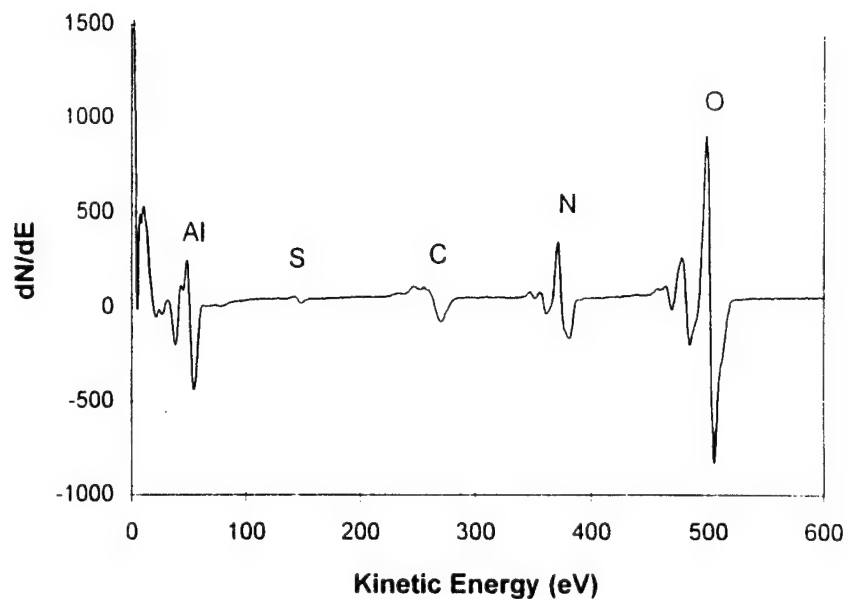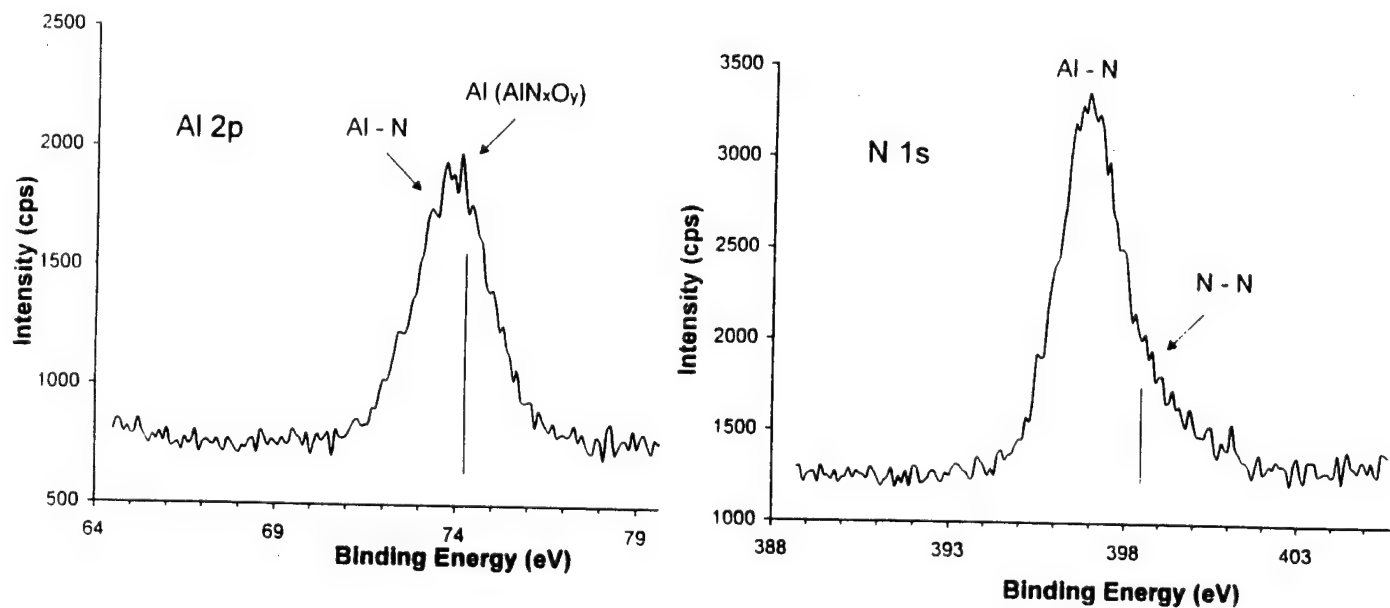

Fig. 23   AES spectrum

Fig. 24   XPS spectra

AlN can be produced via surface reaction using ammonia and aluminum-containing metal-organic precursor at elevated temperatures. DMEAA precursor employed in the present study seems to be working because of low dissociation energy of the aluminum-amine bond and stability of amine ligand, allowing the reaction to be carried out at temperatures much lower than those typically needed for AlN thin film deposition. For the atomic layer growth of AlN, the first step of the reaction involves the dissociation of DMEAA molecules by breaking aluminum-amine bonds, leaving AlH_3 species adsorbed on the WS_2 surface. Although the adsorption sites, nor chemical interaction between dissociated species with the substrate, are not known, it is likely to form two dimensional layer of DMEAA dissociated species, of which periodicity is determined by the WS_2 lattice constant. Subsequent exposure/reaction to NH_3 forms Al-N bonds, constructing AlN lattice structure. Because of close proximity of the lattice constant for WS_2 and AlN, the lattice constant for the first AlN layer may not be distorted, making subsequent growth of AlN unstrained. These steps are schematically illustrated in Fig. 25.
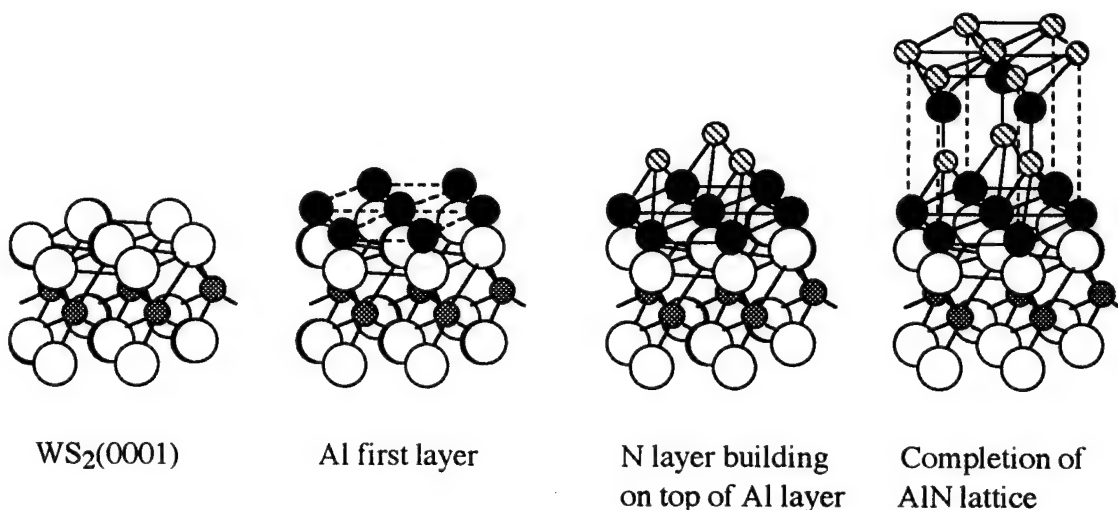

| WS$_2$(0001) | Al first layer | N layer building on top of Al layer | Completion of AlN lattice |

Fig. 25 Schematically illustrated model for AlN lattice growth on WS_2(0001) surface.

Relatively high deposition rate for AlN growth was found for sapphire substrates[ref]; this is because the propensity of DMEAA molecules to form involatile solid with oxygen is relatively high. In the present case, however, the deposition rate was found to be a several factor slower than the sapphire case. This is partly understood that there is little or no oxygen on WS_2 thin film in our case, therefore the initial reaction that is necessary to initiate the subsequent reaction with NH3 is not efficient as the sapphire case. Although a sulfur is among the family including an oxygen, the chemistry of DMEAA to sulfur may be different from that to oxygen. This is why the deposition conditions found for WS_2 case are very different from what was found for the sapphire case.

D.4 MICROSTRUCTURE OF AlN THIN FILMS

Microstructure of AlN thin films was critically dependent on the surface morphology of WS_2 thin films. From a vast amount of data, two cases of the AlN deposition on with different WS_2 surface morphology were chosen to demonstrate the effect.   The first WS_2 substrate was primarily c(=) type, in which the WS_2 basal planes stay parallel to the substrate , whereas the second substrate was c(//) type.   After the AlN growth, cross-sectional specimens were prepared and observed by TEM.

Shown in Fig 26 are the cross sectional images of (a) AlN on WS_2 (20nm thick)/Si and (b). AlN on WS_2 (200nm thick)/Si.   As seen from the images, remarkably different crystal morphology of AlN thin films were apparent. It is apparent form the micrographs that the AlN thin films were not uniformly grown on the c(//)-WS_2 substrate, whereas relatively uniform growth of the AlN thin films occurred on c(=)-WS_2 substrate. For both cases, the AlN thin films were   grown in columnar fashion with their c-axis nearly perpendicular to the substrate. It should be noted that the specimen (a) was relatively easily broken into two parts through WS_2 intermediate layers, whereas the specimen (b) had a stronger interfaces. Because of the differences in mechanical strength at the interfaces, sample preparation was varied from sample to sample.

ALG Grown AlN Thin Films on WS_2(~20nm-thick)/Si
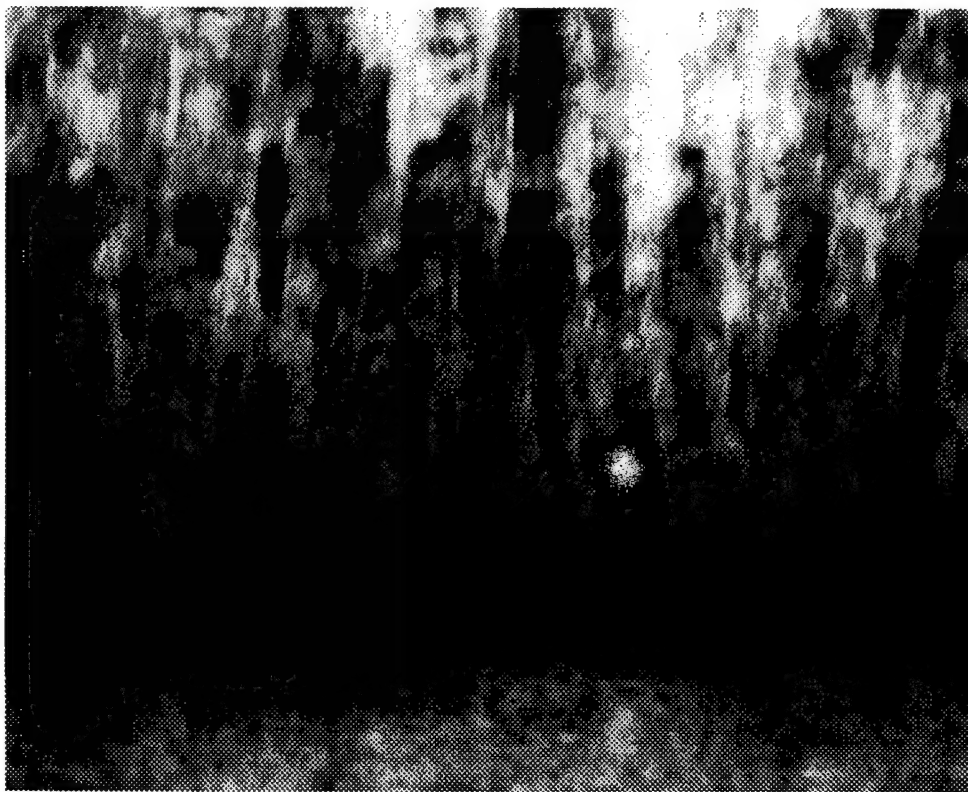
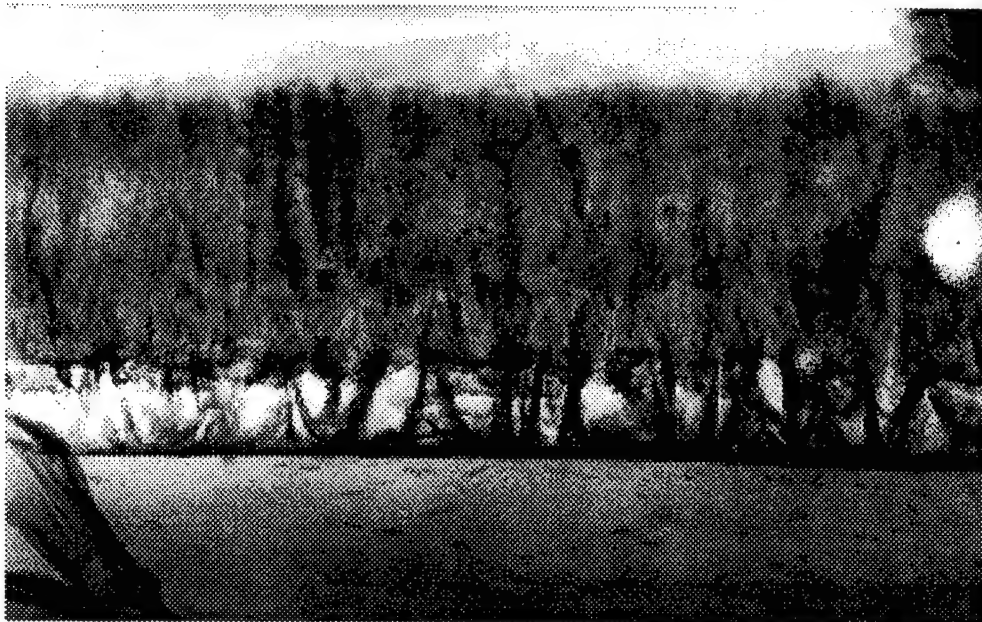## ALG Grown AlN Thin Films on WS$_2$(~200nm-thick)/Si

Fig. 26   Cross sectional TEM images of (a) AlN on WS$_2$ (20nm thick)/Si and (b). AlN on WS$_2$ (200nm thick)/Si

A plan view TEM micrograph along with selected area diffraction (SAD) obtained from AlN thin film is shown in Fig. 27. In this examination, the AlN/WS$_2$/Si specimen was mechanically dimpled to thin section from the Si substrate side, followed by Ar ion milling to obtain electron transparent specimen. Thin film grains with an average size of 90-100Å were uniformly distributed throughout the sample. SAD formed a powder like patter of diffraction. Surface morphology was also observed by AFM in a contact mode. Typical structure of the AlN thin films is shown in Fig. 28.
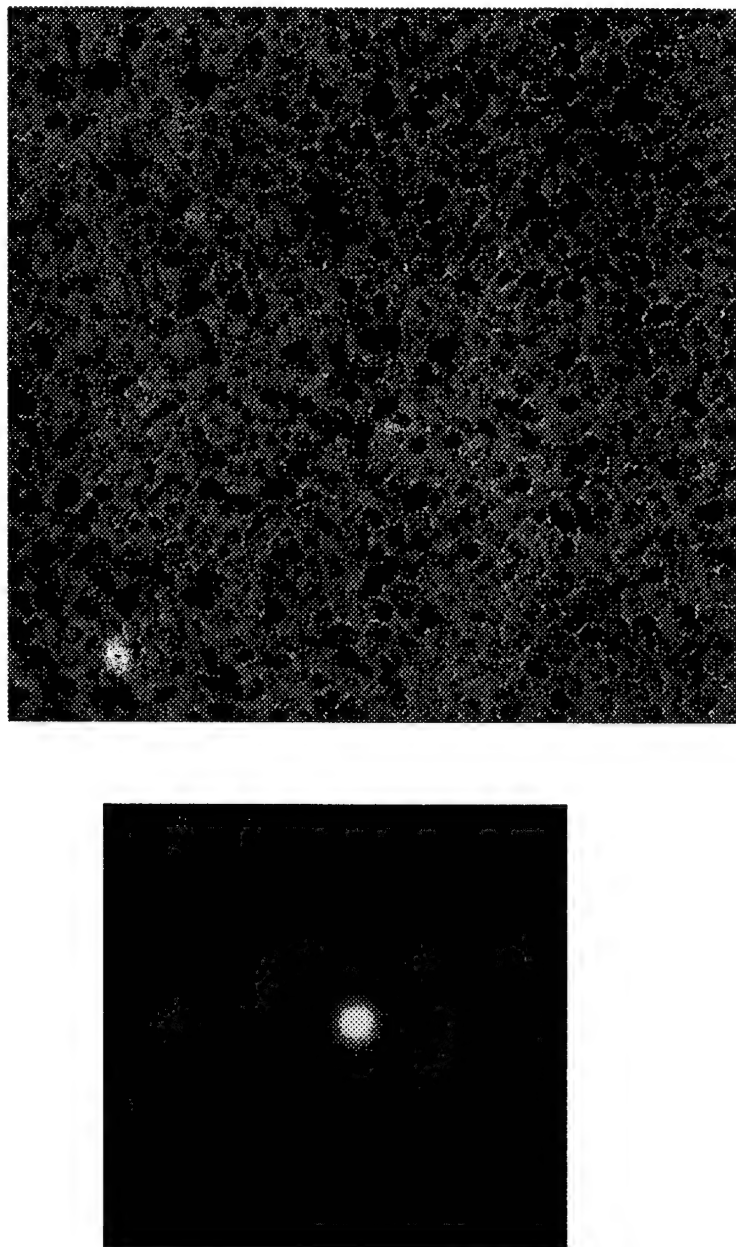
Fig. 27   Plan view TEM image from AlN thin film, and corresponding selected area
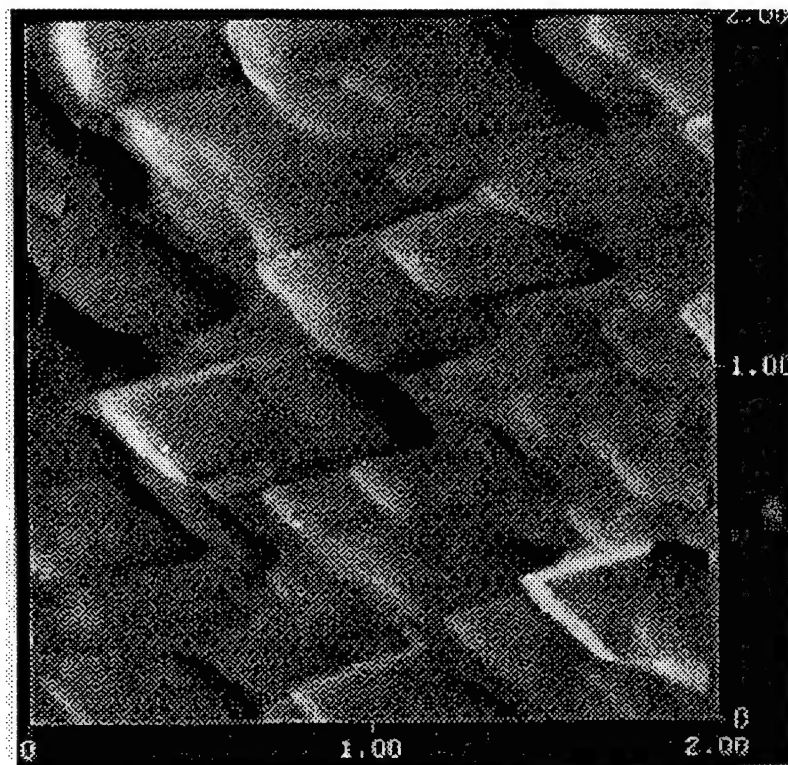diffraction pattern

Fig. 28   Surface morphology of AlN thin films observed by AFM

A close look at AlN thin film structure from (a) is shown in Fig 29. It was found that several columnar AlN crystals were lined up with their c-axis nearly perpendicular to the substrate. SAD examination in order to identify the crystallographic orientation of the individual columnar grain since the aperture was too large to look at individual columnar grain. Scanning Transmission Electron Microdiffraction technique was thus employed to evaluate the crystallographic orientation of the columnar structure. The results are also shown in Fig. 29. It was found that a series of (000k), where k=1, 2, 3 - -, spots were lined up in the direction that the columnar structure developed. Probing the microdiffraction from column to column, growth direction was misaligned within a few degrees.

In order to further study the atomic structure, an HREM image was obtained from the AlN thin film mentioned above, and the micrograph was shown in Fig. 30. Experimental images shown in Fig.30(a) contained high frequency noises. Filtered image after removal of the high frequency noises from the image is shown in (b). Fast Fourier Transform (FFT) technique was then applied to obtain diffraction pattern in (c). This experimental pattern was well matched to one calculated diffraction pattern of AlN with the zone axis aligned to the [-12-10] direction. Using this information, the AlN lattice image was simulated, and compared with the filtered image. A series of image simulations are shown in Fig. 31, from which most matched pattern is shown in Fig. 30(d). While experimental images contains fair numbers of defects, including stacking faults, a reasonably good

-40-

match between experimental and computational images was obtained. Knowing the fact that the growth was made at 735 K, this was the first observation of the lattice image by HREM.
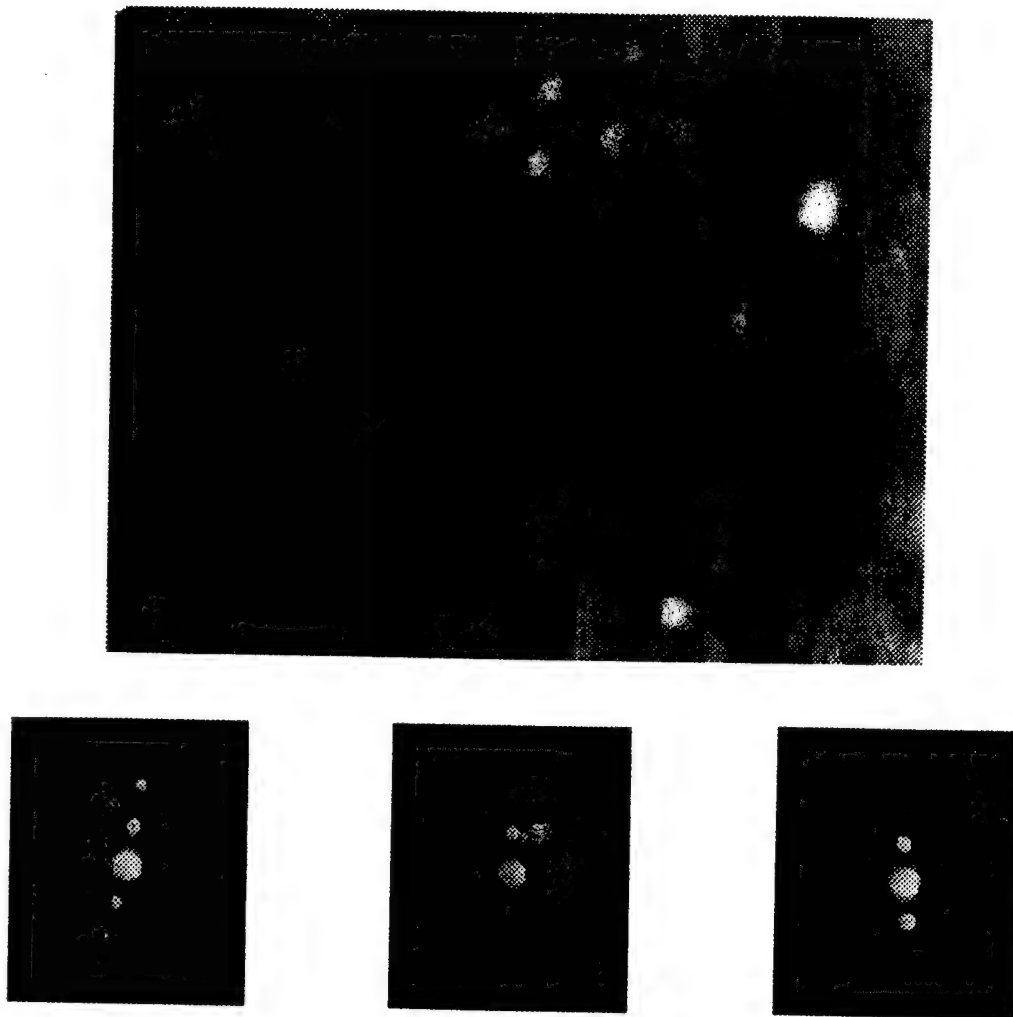
AlN(ALG)/WS$_2$(MOCVD-20nm)/Si

Fig. 29   Cross sectional TEM image from AlN thin films grown on WS$_2$(20nm) thin film substrate, and STEM microdiffraction patterns from each columnar grains.
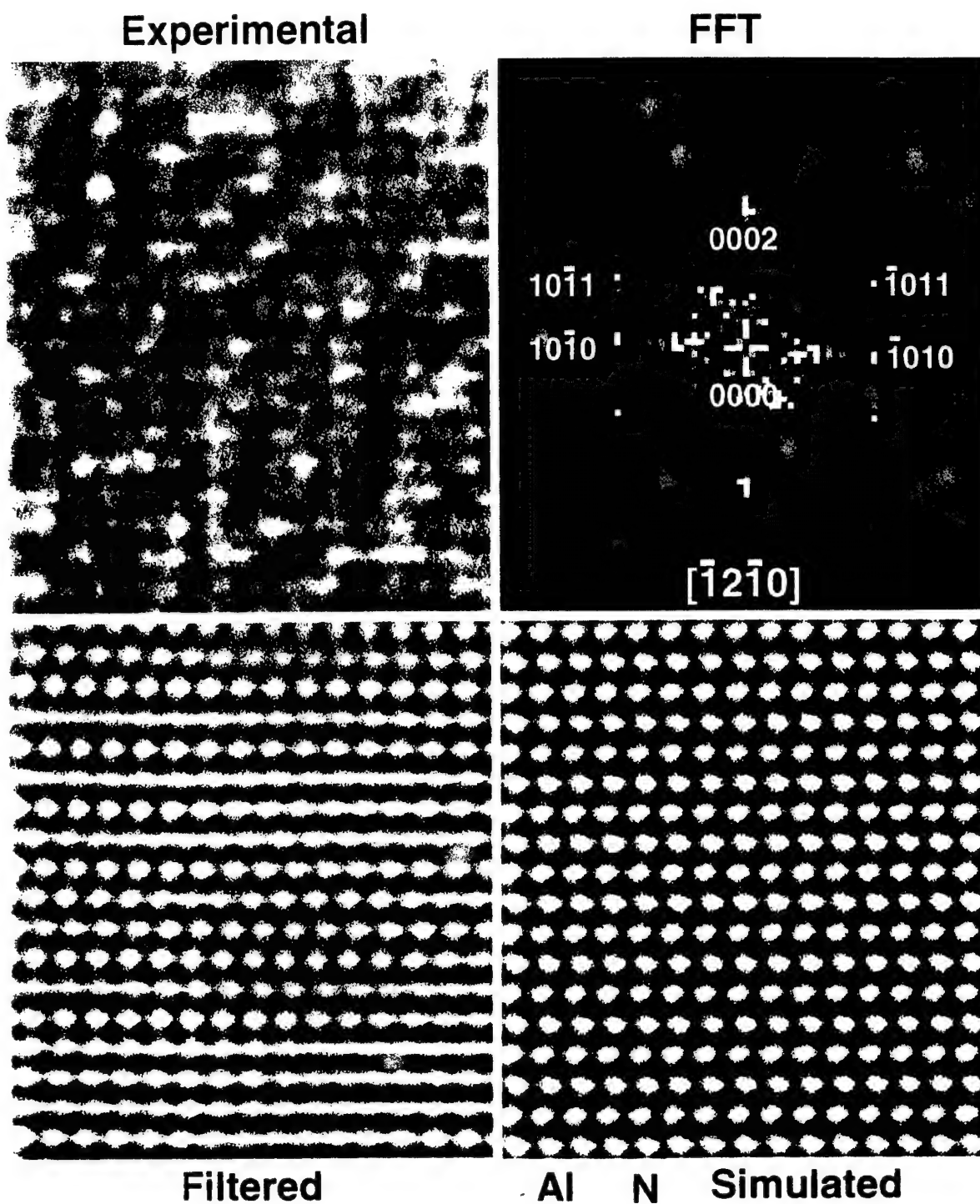
Fig. 30 HREM image obtained from the AlN thin film (a) unfiltered experimental image, (b) filtered image, (c) FFT image and (d) simulated image
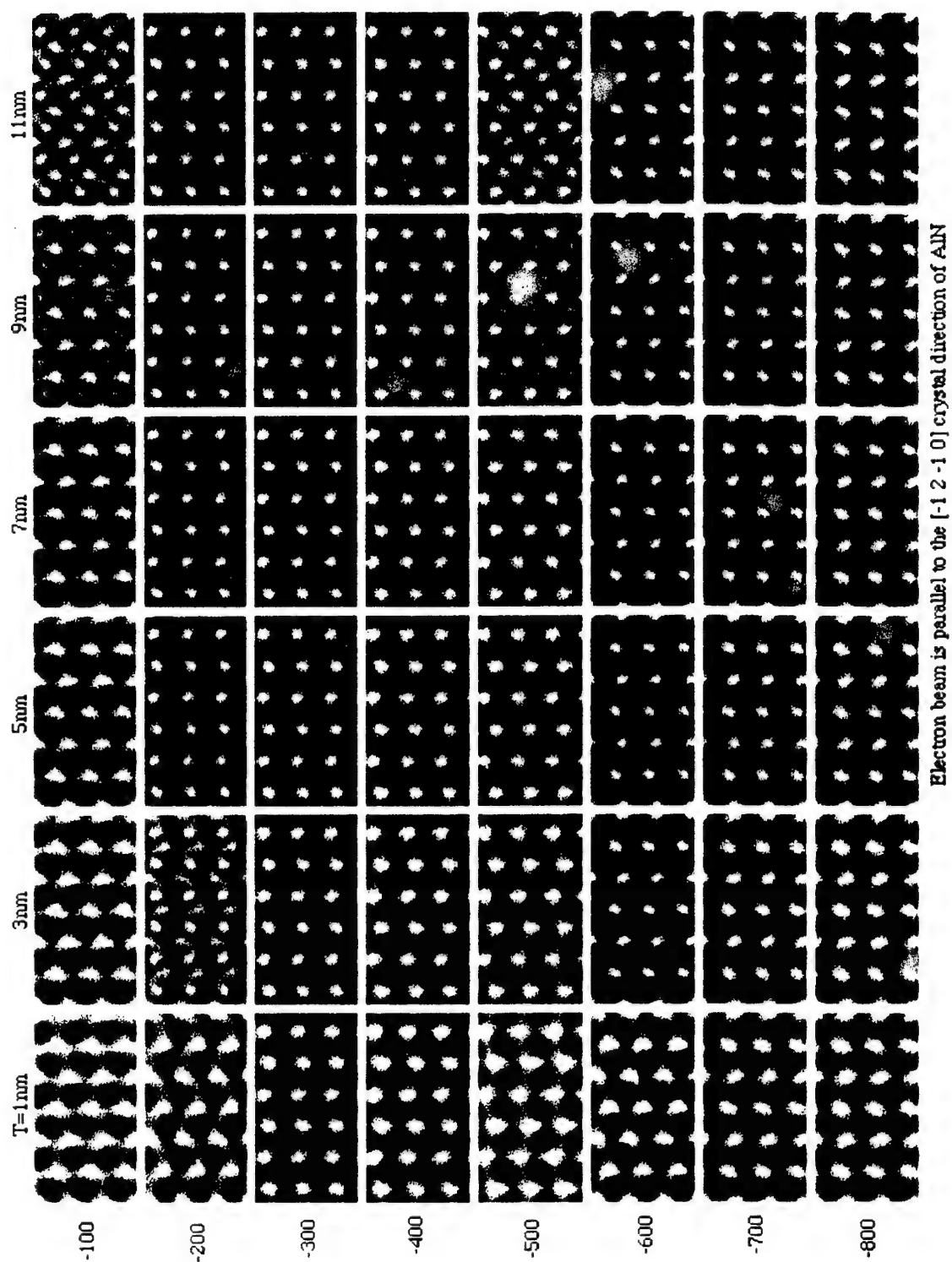
Fig. 31   A series of image simulation by changing defocus condition and sample
thickness.

E. DEMONSTRATION OF THE VAN DER WAALS LIFT-OFF

Our original goal was to fabricate a self-standing AlN thin films after removal through van der Waals layers. This was demonstrated by mechanically removing AlN thin films from the substrate through WS_2 layers. A sticky tape was applied to the AlN thin film side, which was peeled off from the substrate. Peeled section was washed in acetone to remove glue from the specimen, transferred to a 600 meshed Cu-TEM grid. Overall image was shown in Fig. 32.

Fig. 32   TEM examination of peeled AlN thin film section.

A portion of "lift-off" AlN thin film specimen was further examined by plan view TEM along with selected area diffraction (SAD) patterns in Fig. 33. Columnar growth of the AlN thin films was directly observed in this micrograph. There are, however, substantial planer defects with in the columns, which are identified as irregular shape of the morphology and un-uniform contrast of the electron image. SAD pattern contains the diffraction spots from WS_2 substrate thin films. This indicates that a part of WS_2 thin films were adhered to the AlN specimen during the lift-off process (see Fig. 1).
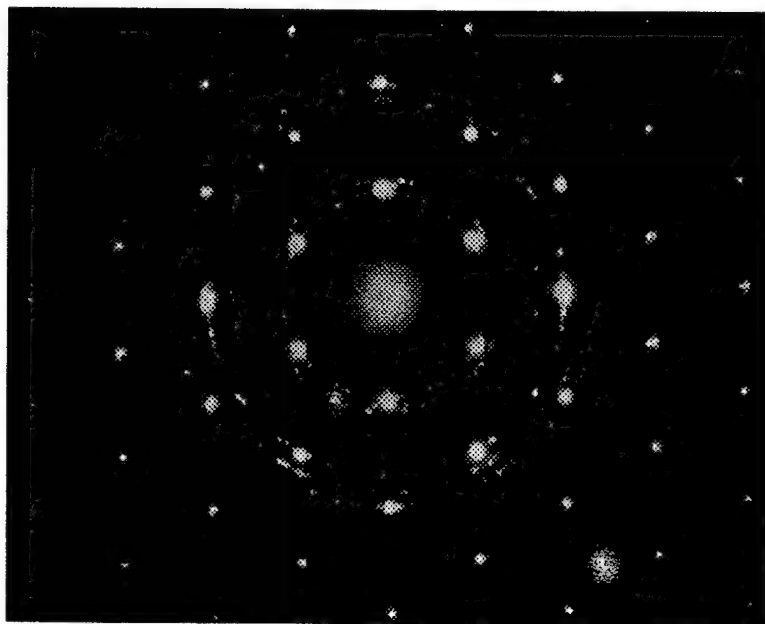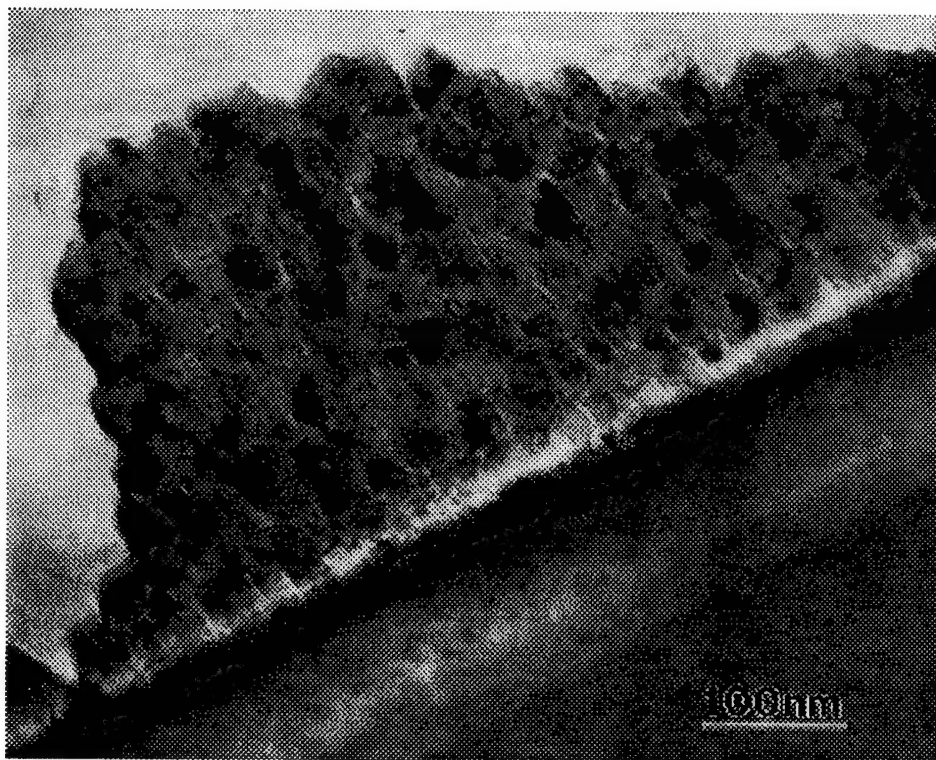
-44-

Fig. 33 A plan view micrograph of AlN thin film after removal from the substrate. SAD pattern showing both AlN and WS$_2$ spots are also shown.

It was shown before that morphology of the WS2 thin film substrate influenced strongly the growth mode of subsequent AlN thin film deposition. Approximately a micron-thick AlN thin film was grown on WS_2 thin film substrates with c(=) orientation. The AlN thin films were removed from the substrates. Shown in Fig. 34 are AlN thin films left over the WS_2/Si substrate.
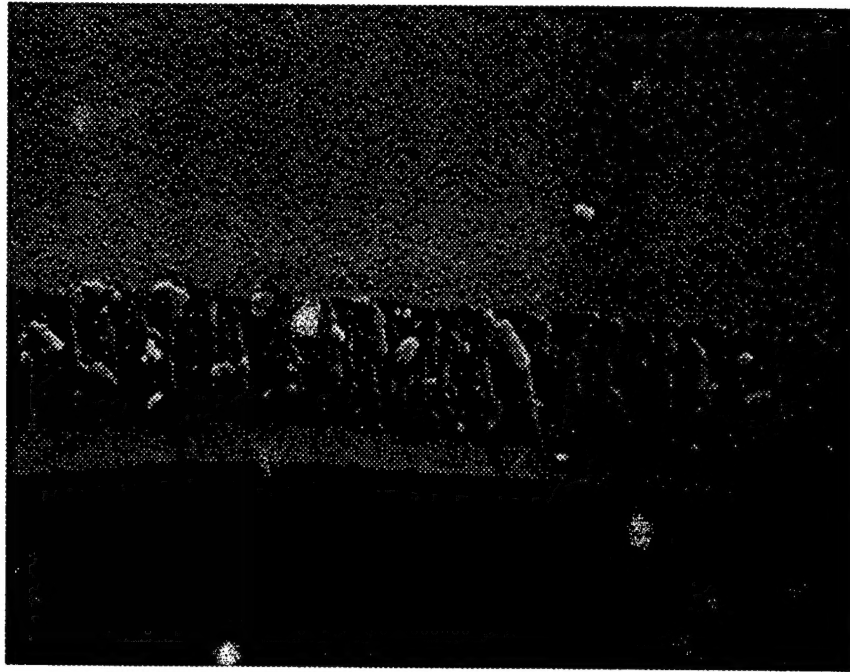

Fig 34. SEM micrographs of AlN thin films grown on c(=)-WS_2 substrate.

IV. CONCLUSION

Tungsten disulfide has been used as a substrate for the growth of aluminum nitride by atomic layer growth mode using the novel precursor combination of dimethylamine-alane (DMEAA) and ammonia (NH_3) has been demonstrate. Close proximity of the lattice constant of WS_2 to those of AlN may lead to a potential application of this materials as a substrate for subsequent growth of AlN, however, the details chemistry for the reaction between first DMEAA molecular layer with WS_2 surface must be worked out in order to develop this process.

Microstructure of AlN thin films was critically dependent on the surface morphology of WS_2 thin films. AlN thin films were uniformly grown on the c(=)-WS_2 substrate, whereas growth of the AlN thin films on c(=)-WS_2 substrate occurred irregularly. For both cases, the AlN thin films were grown in columnar fashion with their c-axis nearly perpendicular

to the substrate. Van der Waals lift-off was demonstrated by mechanically removing AlN thin films from the substrate through WS_2 layers. Inability to fabricate thick enough specimens of the AlN thin film by ALG technique, however, limited further investigation of this process.

V. PERSONNEL SUPPORTED

Faculty	Fumio S. Ohuchi Professor of Materials Science and Engineering
Graduate Student	Kaveh Adib
Visiting Scholar	J. W. Chung (from Hanyang University, Korea)

VI. PUBLICATIONS

"Metalorganic Chemical Vapor Deposition of Layered WS_2 Thin Films", J-W. Chung, and F. S. Ohuchi, J. Crystal Growth, 186 (1998) 137-150.

"Deposition of AlN on WS_2(0001) by Atomic Layer Growth Process"
J.W. Chung and F. S. Ohuchi,
Materials Research Society , Proceeding (1997)

"Raman Scattering and High Resolution Electron Microscopy Studies of MOCVD-WS_2 Thin Films", J.W. Chung, Z.R. Dai and F. S. Ohuchi, *Thin Solid Films*
Submitted in December-1997; currently under review

"Unusual Polytype of WS_2 Single Crystals Prepared by Iodine Vapor Transport"
J-W. Chung, Z. R. Dai, J. MaClaine and F. S. Ohuchi, *Journal of Crystal Growth:*,
Submitted in March-1998; currently under review

VII. INTERACTIONS/TRANSITIONS

VII.1 PARTICIPATION/PRESENTATIONS AT MEETINGS, CONFERENCES

• Materials Research Society -Spring Meeting (April-1996) San Francisco, Cal.

• 1996 TMS meeting on Electronic Materials, University of California, Santa Barbara, Cal., June 24-26, 1996   Presentation: Atomic Layer Growth of AlN

- 1997 Spring Materials Research Society meeting, San Francisco, Cal

- 1997 American Vaccum Society National Meeting, Philadelphia, PA

VII.2 CONSULTATIVE AND ADVISORY FUNCTIONS TO OTHER LABORATORIES

Dr. Mike Alexander   Rome Research Laboratory (USAF-AFMC)
Dr. Nil Fernelius   Wright Laboratory (USAF-WP AFB)
Wright Laboratory (tribology research group)
Dr. Jacques I. Pankove   Astralux, Inc.

We developed the synthesis route for WS_2 thin films using metalorganic chemical vapor deposition (MOCVD). Wright Laboratory is currently investigating WS_2 thin films fabricated by laser ablation technique for tribological applications. MOCVD has particular advantages over the other methods in fabricating thin film coatings in term of their uniformity, non-directionality, and fast deposition. We are currently establishing research collaboration with the tribology research group of the Wright Laboratory in WP-AFB.

VIII NEW DISCOVERIES, INVENTIONS, OR PATENT DISCLOSURES
Deposition conditions for WS_2 using $W(CO)_6$ and H_2S have been identified.

IX HONORS/AWARDS
None

X MARKINGS
None

XI. REFERENCES

1. H. Guernoc, US Govt. Rept. 37 101A AD265121 (1961).
2. R. Motsjcje, in : Crystal Growth, Ed. H. S. Pier (Permagon, Oxford, 1967)
3. H.Schafer, Chemical Transport Reactions, Academic Press, New York, 1964, p.55.
4. M. Regula, C. Ballif, J. H. Moser and F. Lévy, Thin Solid Films, 280 (1996) 67.
5. M. Genut, L. Margulis, R. Tenne and G. Hodes, Thin Solid Films, 219 (1992) 30.
6. J. S. Zabinski, M. S. Donley, N. T. McDevitt and S. V. Prasad, J. Mater. Sci., 29(1994) 4834.
7. W. L. Holstein, Prog. Crystal Growth and Charact., Ed. by J. B. Mullin, (Pergamon Press Ltd., 24, 1992) p.168.
8. X-ray powder diffraction JCPD file No 08-0237.

9. N.T. McDevitt, J.S. Zabinski and M.S. Donley, Thin Solid Films, 240 (1994) 76.

10. T. Sekine, T. Nakashizu, K. Toyoda, K. Uchinokura, and E. Matsuura, Solid State Comm., 35 (1980) 371-373.

11. A. Cingolani, M. Lugara and G. Scamarcio, Il Nuovo Cimento, 11D, N.3 (1989) 455.

12. C. Sourisseau, F. Cruege and M. Fouassier, Chem. Phys., 150 (1991) 281.

13. L. Rapoport, Y. Bilik, Y. Feldman, M. Homyonfer, S. R. Cohen, R. Tenne, Nature. 387(6635) (1997) 791.

14. D.J. Cebula, R. K. Thomas and J.W. White, Clays Clay Miner., 29 (1981) 241.

15. J. Moser and F. Levy, J. Mat. Res., 8 (1993) 206.

16. W.Y. Lee and K. L More, J. Mat. Res., 10(1) (1995) 49.

17. M. Regula, C. Ballif, J. H. Moser and F. Lévy, Thin Solid Films, 280 (1996) 67.

18. W.Y.Lee, W. J. Lackey and P.K. Agarawal, J. Am. Ceram. Soc., 74, 1821 (1991)

19 H. J. Kim, Y. Egashira and H. Komiyaman, Appl. Phy. Lett., 59,2521 (1991), K.G. Nickel, R. Riedel and G. Petzow, J. Am . Ceram. Soc., 72, 1804 (1989)

20. Y.G. Roman and A. P. M. Adiaasen; ,Thin Solid films, 169, 241 (1989)

21. Z. J. Yu, J. H. Edgar, A.U. Ahmed and A. Rys, J. Electrochem. Soc. 138, 196 (1991).

22. T.L. Tansley, L. Xin and M . Yanhua, Thin Solid rilms, 163, 255 (1988)

23. X. Li and T. L.Tansley, J. Appl. Phy., 68, 5369 (1990).

24. S. Yoshida, S. Misawa, Y. Fujii, S. Tanaka. H. Hayakawa, S. Gonda and A. Itoh, J. Vac. Sci. Technol. 15, 990 (1979), H. Baier and W. Monch, J. Appl. Phys., 68, 586 (1990); Z. Sitar, M.J.Paisley, B. Yan, J. Ruan, W.J. Chyoke and F.R.F Davis, J. Vac. Sci. Technolo. B8, 316 (1990).

25. Other techniques include: ion beam deposition, ion implantation, electron bea mdeposition, grow discharge sputter deposition, reactive ion planting deposition and magnetron sputtering deposition.

26. M. E. Bartram, T.A. Michalske, J.W. Rogers Jr., and T. M. Mayer, Chem. Mater., 3, 953 (1991); T. Mayer, J. W. Rogers Jr., and T.A. Mchalske, Chem. Mater. 3, 641 (1991), D. C.Bertolet and J.W. Rogers Jr., Chem. mater. 5, 391 (1993), M.E.Bartram, T.A. Michalske, J.W. Rogers Jr., and R.T. Paine, Chem. Mater., 5, 1424 (1993); D.C. Bertolet, H. Liu and J.W. Rogers Jr.,Chem. Mater.5, 1814 (1993).